UNIVERSITY OF LATVIA

Summary of Doctoral Thesis

Anda Ābola

MERCURY AND ARSENIC CONTAINING LIGHT SOURCES AND THEIR USAGE FOR ATOMIC ABSORPTION SPECTROSCOPY

Riga 2024

UNIVERSITY
OF LATVIA

FACULTY OF PHYSICS, MATHEMATICS AND OPTOMETRY

Anda Ābola

MERCURY AND ARSENIC CONTAINING LIGHT SOURCES AND THEIR USAGE FOR ATOMIC ABSORPTION SPECTROSCOPY

SUMMARY OF THE DOCTORAL THESIS

Submitted for the degree of Doctor of Physics and Astronomy

Subfield: Laser Physics and Spectroscopy

Riga 2024

Doctoral thesis have been carried out at the Institute of Atomic Physics and Spectroscopy, University of Latvia, during the time period from 2011 to 2023.

The work was created with the financial support of the following projects:
- "Strengthening of the capacity of doctoral studies at the University of Latvia within the framework of the new doctoral model" (No 8.2.2.0/20/I/006, ESF)
- "Mercury Contamination in Wild Birds in Latvia: Current Patterns and Reconstruction of Previous Trends" (No lzp-2020/1-0005, LZP)
- "Spectrometric techniques for detection of heavy metal contaminants" (ESF)
- Global Mercury Observation System (GMOS) (EU 7th Framework)
- Atomic physics and medical physics; Atomic physics, optical technologies and medical physics (UL IAPS)

The thesis consists of introduction, 6 chapters, conclusions, a reference list and 4 appendices.

Form of the thesis: dissertation in Physics, Laser Physics and Spectroscopy

Supervisors:

Dr. Phys. **Atis Skudra**, leading researcher (Institute of Atomic Physics and Spectroscopy, UL)

Dr. Phys. **Gita Rēvalde**, professor (Faculty of Materials Science and Applied Chemistry, RTU), leading researcher (Institute of Atomic Physics and Spectroscopy, UL)

Reviewers:

1) Dr. phys. **Andris Jakovičs**, University of Latvia
2) Dr. habil. phys. **Andris Ozols**, Riga Technical University
3) Dr. phys. **Georges Zissis**, Toulouse III – Paul Sabatier University, France

The thesis will be defended at the public session of the Doctoral Committee of Physics and Astronomy, University of Latvia on January 26, 2024 at 15:00, at Science House of UL, Jelgavas str 3.

The thesis and its summary are available at the Library of the University of Latvia, Raina Blvd. 19.

Chairman of the Doctoral Committee: Dr. phys. **Gunta Krūmiņa**

Secretary of the Doctoral Committee: **Sintija Siliņa**

© Anda Ābola, 2024
© University of Latvia, 2024

ISBN 978-9934-36-136-4
ISBN 978-9934-36-137-1 (PDF)

Abstract

Increasing attention is given to environmental pollution and its impact on the health of the living organisms and the environment itself. Atomic absorption spectroscopy is a well–known analytical method for measuring environmental pollution. However, with growing demands for detecting lower and lower concentrations of toxic elements and making the equipment more mobile, there is a need to further develop it. One of the approaches to achieve this is by producing improved light sources.

The High–Resolution Spectroscopy and Light Source Technology Laboratory at the Institute of Atomic Physics and Spectroscopy of the University of Latvia is engaged in the development and research on high–frequency electrodeless light sources. To improve light sources and optimize their operation, spectroscopic studies are required.

In the doctoral thesis, lamps with arsenic and mercury fillings, manufactured in the laboratory, were studied. The dependence of the resonance spectral line intensities of As at 189.0 nm, 193.8 nm, and 197.3 nm and Hg at 253.7 nm on the excitation generator power, frequency, and operating mode was investigated. Lamp stability, self–absorption, and temperature were evaluated. Periodic intensity changes, self–modulation, were observed in arsenic lamps, and their period was calculated. In addition to high–frequency electrodeless lamp radiation studies, a comparison with commercially available hollow cathode lamps was also performed.

The main conclusions obtained are as follows: getter addition improves lamp performance, lamp radiation fluctuations do not exceed a 2% limit, the temperature of As lamps is approximately 950–1250 K, and the optimal operating power is around 14 W due to self–absorption. Self–modulation depends on the lamp voltage and its period decreases at higher voltage values. It was also concluded that the best results for Hg capillary lamps are achieved when the capillary is placed horizontally, spherical Hg lamps are recommended to be operated in the E–discharge mode, and As lamps in the H–discharge mode.

In addition to spectroscopic measurements, Hg concentration determination was carried out in the eggshells and feces of black storks, as well as in lake water samples, using an atomic absorption spectrometer with Zeeman background correction. The total number of analyzed samples exceeded 1,000 samples from more than 130 nesting sites across Latvia. The thesis compares Hg concentrations in eggshells and membranes, determining that the average concentration in eggshells is 16 ng/g, in membranes – 202 ng/g, with its ratio of eggshells to membranes being $\approx$11 times. Differences in Hg concentrations in the feces of adult storks and young birds were analyzed, as well as its changes from 2019 to 2022. Water sample measurements were conducted as part of an inter–laboratory study. The obtained results match well with the results obtained by other participants.

Main abbreviations and notations

Frequently encountered abbreviations:

AAS – atomic absorption spectroscopy, also spectrometer
HFEDL – high–frequency electrodeless lamp
HCL – hollow cathode lamp
UV – ultraviolet

Most frequently encountered symbols and physical constants:

A – absorbance
A_{ik} – transition probability
C – concentration
E_{rot} – energy
I_0 – incident light intensity, also intensity at the center of spectral line
I_ν – transmitted light intensity
I_{max} – maximal intensity of spectral line
I_{ik} – spectral line intensity, occurring in transition between i and k levels
i – excited state
K_ν – absorption coefficient
k – ground state
N_i, N_k – concentration of atoms
T^{rot} – rotational temperature
λ, λ_{ik}– wavelength
ν, ν_{ik} – frequency
$h = 6,62 \cdot 10^{-34} J \cdot s$ – Planck's constant

Contents

Introduction

Nowadays, increasing attention is being paid to environmental pollution, and there is a growing understanding of the effects of various toxic and harmful substances on both the environment and living organisms [1]. This has led to a growing need to detect toxic elements at very low concentrations, which are often close to the background concentrations of these elements in the environment [2]. Therefore, new methods and instruments for pollution measurement are being developed to achieve these goals.

Atomic absorption spectroscopy is a relatively old but still popular analytical method for the quantitative determination of various elements [3, 4]. Its origins can be traced back to the 1950s when Alan Walsh published a paper describing the use of atomic absorption spectra for chemical analysis [5]. Due to its high sensitivity, atomic absorption spectroscopy forms the basis of many standard methods [4], such as EPA Method 245.1 for the determination of mercury [6].

The actuality of the problem

The importance of this work is associated with the increasing need to determine very low concentrations (from a few nanograms to a few micrograms per liter, gram, or cubic meter) of various toxic elements. As the requirements for the achievable results grow, the challenges that the chosen analytical methods have to overcome also increase. These challenges include improving detection limits, reducing measurement times to allow real–time analysis, and minimizing the size of instruments to ensure their portability [7, 8].

One of the key elements that determine the sensitivity and performance of atomic absorption spectrometers is the light source. Typically, in atomic absorption spectroscopy, high–frequency electrodeless lamps or hollow cathode lamps are used as line spectrum light sources.

The Laboratory of High–Resolution Spectroscopy and Light Sources Technology at the Institute of Atomic Physics and Spectroscopy of the University of Latvia (UL IAPS) has accumulated significant experience in the production of high–frequency electrodeless light sources (e.g., [9–11]) and continues to actively research them. Advancements in technology have made it possible to create lamps that produce more intense radiation and have longer lifetimes, as well as to improve the shape and spectral composition of lamps, and to reduce their size [12]. To achieve this, spectroscopic studies are needed to obtain information that can be used to further improve and adapt manufacturing technologies and optimize the operating conditions of the produced light sources. Finding the best parameter combination is a complex task since the emitted spectral lines of the light source must be intense, narrow, and non–self–absorbed. The work focuses on high–frequency electrodeless lamps containing mercury and arsenic, as it is problematic to produce hollow cathode lamps with these elements [13].

Arsenic and mercury are well–known toxic elements. Arsenic is ranked first on the 2022 Substance Priority List by the Agency for Toxic Substances and Disease Registry (ATSDR) [14]. This list compiles substances considered hazardous to human health based on their known or anticipated toxicity and prevalence. Arsenic is widely distributed in the Earth's crust and groundwater [15] and enters the environment through human activities [16]. The long–term ingestion of toxic elements in small doses through food and water can lead to chronic health problems, making it important to detect even low levels of contamination.

Mercury is ranked third on the ATSDR's Substance Priority List [14]. The need to detect mercury at levels close to background concentrations (0.0015 μg/m^3 in the air [17], 60 μg/kg in soil [18], up to 2 μg/l in water [19]) is associated with several factors. First, it is related to the process of mercury methylation, mainly occurring in aquatic environments [20]. Second, it is linked to the bioaccumulation and biomagnification of mercury in the food chain [21], where even low concentrations of mercury can accumulate to levels hazardous to health [22].

In addition to practical applications in atomic absorption spectroscopy, quantum standards, goniometers, and lately also in disinfection [23,24], high–frequency electrodeless light sources, being low–temperature plasma sources, are used for fundamental plasma process research and plasma–surface interaction studies [P9].

The assessment of Hg as a toxic element distribution in Latvia has not been conducted. Yet it was found that there is a significant amount of mercury in the blood of endangered bird species in Latvia, black storks (*Ciconia nigra*) [25]. Therefore, this work also includes measurements of Hg concentrations in natural samples – water and black stork eggshells and feces – using an atomic absorption spectrometer with a high–frequency electrodeless lamp containing mercury.

Over the past thirty years, the number of breeding pairs of black storks in Latvia has significantly decreased [26]. Therefore, one of the questions related to mercury measurements in black storks is whether mercury concentration could affect their reproductive success. If birds ingest large amounts of mercury, they may develop various health problems, as mercury is a well–known neurotoxin. Reproductive problems may also arise, and at very high concentrations, mortality can occur [27]. Since black storks primarily feed on fish [28], they are at a higher risk of mercury intake [29]. Eggshells and feces as samples for measurements were chosen because of their availability, as their collection is non–invasive and minimally affects the birds, as they are not disturbed [P1]. These are important conditions for choosing biological samples for analysis, especially if the studied species, such as black storks in Latvia, are endangered [26].

Simultaneously, the data obtained in mercury concentration measurements, when correlated with geographical and geological data, will enable the mapping of mercury pollution in Latvia.

The doctoral dissertation consists of an introduction, six chapters, conclusions, four appendices, and a list of references. It includes 68 figures and 9 tables.

The doctoral dissertation is reflected in 11 publications in scientific journals and conference proceedings, as well as 18 abstracts for international conferences.

Scientific novelty

- Spectral lines of arsenic in the far UV region (189 nm, 194 nm, 197 nm) and their profiles in high–frequency discharges were studied.
- The stability of over time of arsenic and mercury high–frequency electrodeless lamps was investigated, and data on fluctuations during the lamp's stable operation were obtained.
- The self–modulation regime in arsenic lamps was studied for the first time, and the influence of lamp manufacturing technology on its occurrence was assessed. The self–modulation period was calculated, and the relationship between self–modulation and changes in line profiles was demonstrated.
- For the first time, the gas temperature in arsenic–containing high–frequency electrodeless lamps was determined using OH rotational band spectra.
- For the first time, the Hg concentration was determined in the eggshells and membranes of protected species – black storks, breeding in Latvia. The Hg levels in eggshells and membranes were compared and the correlation of Hg concentration in them was assessed. Samples collected over 20 years from black stork nesting sites all across Latvia were used in the study.
- Within the scope of the work, the mercury concentration was determined for the first time in the feces of black storks, who are breeding or have hatched in Latvia. A comparison of mercury concentrations in the feces of adult birds and chicks was conducted for the period from 2019 to 2022.

Aims of the work

1. To investigate arsenic and mercury containing light sources in order to optimize their performance for use in atomic absorption spectrometers. Light sources are manufactured at UL IAPS Laboratory of High–Resolution Spectroscopy and Light Sources Technology.
2. To develop methodology for mercury concentration measurements in biological and environmental samples, by using atomic absorption spectrometer with capillary Hg light source and Zeeman background correction. Approbate the method by performing Hg concentration measurements in eggshells and feces of black storks, and water samples.

Tasks of the work

1. To perform intensity measurements of UV spectral lines of arsenic and mercury in high–frequency electrodeless light sources produced at the UL IAPS Laboratory of High–Resolution Spectroscopy and Light Source Technology, depending on their operational and manufacturing conditions.
2. To investigate the stability of As and Hg high–frequency electrodeless lamps over time and to obtain data on fluctuations in the lamps' stable regime.

3. To compare the impact of excitation generators on As high–frequency electrodeless lamp radiation.
4. To determine the gas temperature in multiple As–containing high–frequency electrodeless lamps using OH rotational spectrum lines.
5. To study the effect of the operating position of capillary on the radiation of Hg capillary lamps.
6. To investigate the spectral lines of Hg high–frequency electrodeless lamps in E and H discharges.
7. To compare the spectra of As and Hg–containing high–frequency electrodeless lamps with hollow cathode lamps.
8. To develop a methodology and conduct mercury concentration test measurements in the eggshells, membranes, and feces of endangered black storks.
9. To develop a methodology and conduct mercury concentration test measurements in water samples.

Theses

1. Between three As resonance spectral lines in the far UV spectrum 189.0 nm, 193.8 nm, and 197.3 nm, the most suitable spectral line for use in atomic absorption spectroscopy is 197.3 nm.
2. The addition of a getter improves the operating parameters of arsenic high–frequency electrodeless lamps, by increasing intensity and enhancing stability.
3. Capillary mercury light sources should be operated with capillary positioned horizontally, while spherical Hg light sources are preferably operated in E–discharge, to avoid self–absorption of spectral lines.
4. Zeeman atomic absorption spectrometer with Hg capillary light source is suitable method for mercury concentration determination in biological and environmental samples. Pyrolitic atomization enables mercury concentration measurements in samples with mercury amounts close to background levels, for example, in eggshells of endangered birds.

Main methods

1. Spectroscopic data registration – light sources' spectra acquisition, by using spectrometers with different spectral resolutions;
2. Spectroscopic data processing and analysis – use of such functions as integration, approximation, fitting, averaging etc.;
3. Atomic absorption spectroscopy with Zeeman background correction – analytical method for mercury concentration measurements;
4. Cold–vapor method – atomization of Hg compounds, using a set of chemical substances;
5. Pyrolitic atomization – atomization of Hg compounds, using pyrolitic combustion.

List of publications and conferences

Publications connected to the theme of the dissertation:

[P1] A. Abola, A. Rimsa, R. Veilande, M. Strazds, G. Revalde. Data correlation of mercury in eggshells and eggshell membranes of wild birds. Engineering for Rural Development (2023), Article Nº TF071. DOI: 10.22616/ERDev.2023.22.TF071

[P2] N. Zorina, A. Abola, A. Skudra, G. Revalde. Study of arsenic resonance spectral lines in far UV region from a HFEDL for usage in Zeeman absorption spectroscopy. IOP conference series: Journal of Physics Vol. 2439 (2023) Article Nº012013. DOI:10.1088/1742-6596/2439/1/012013

[P3] A. Abola, Z. Brike, G. Revalde, R. Veilande, K. Rancane, A. Skudra, M. Strazds. Determination of Hg in Biological Samples of Black Storks by Zeeman Atomic Absorption Spectrometry. Imaging and Applied Optics Congress 2022, Technical Digest Series (Optica Publishing Group, 2022), paper JW2A.20. DOI:10.1364/3D.2022.JW2A.20

[P4] A. Abola, M. Strazds, Z. Gavare, R. Veilande. Assessing mercury pollution using black stork eggshells. Proceedings of the 13th International Scientific and Practical Conference Environment. Technology. Resources, Vol. 1 (2021), p. 12 – 16. DOI:10.17770/etr2021vol1.6528

[P5] N. Zorina, A. Skudra, G. Revalde, A. Abola. Study of As and Tl high-frequency electrodeless lamps for Zeeman absorption spectroscopy, Proceedings of SPIE, Vol. 11585, Biophotonics–Riga 2020, Article Nº115850B (2020); DOI:10.1117/12.2580856

[P6] N. Zorina, A. Skudra, G. Revalde, A. Abola. Studies of Thallium Line Spectra in Thallium – Mercury Discharge. IOP Conference Series: Journal of Physics Vol.1289, Nº 1 (2019). Article Nº 012044. DOI:10.1088/1742-6596/1289/1/012044

[P7] E. Bogans, J. Skudra, A. Svagere, Z. Gavare. Analysis of Mercury Pollution in Air in Urban Area of Riga Using Atomic Absorption Spectrometry. W. Leal Filho, A.Ūbelis, D.Bērziņa (eds), Sustainable Development, Knowledge Society and Smart Future Manufacturing Technologies. World Sustainability Series. Springer, Cham. (2015), p. 219 – 228. DOI:10.1007/978-3-319-14883-0_15

[P8] Z. Gavare, A. Svagere, R. Zvejnieks, A. Skudra. The investigation of different discharge modes in high–frequency argon–zinc discharge. Romanian Journal of Physics, Vol. 59, Nº 5 – 6 (2014), p. 561 – 569

[P9] E. Gavars, A. Svagere, A. Skudra, N. Zorina, R. Poplausks. Measurements of SiO_2 glass surface parameters by methods of microscopy. IOP Conference Series: Materials Science and Engineering, Vol.38, Nº 1 (2012), Article Nº 012043. DOI:10.1088/1757-899X/38/1/012043

[P10] E. Bogans, Z. Gavare, A. Svagere, R. Poikane, J. Skudra. Mercury Pollution Exploration in Latvia with High–Sensitivity Zeeman Atomic Ab-

sorption Spectrometry. Environmental and Climate Technologies, Vol. 7 (2012), p. 39 – 45. DOI:10.2478/v10145-011-0026-y

[P11] Z. Gavare, A. Svagere, M. Zinge, G. Revalde, V. Fyodorov. Determination of gas temperature of high–frequency low–temperature electrodeless plasma using molecular spectra of hydrogen and hydroxyl-radical. Journal of Quantitative Spectroscopy and Radiative Transfer, Vol. 113, Nº 13 (2012), p. 1676 – 1682. DOI:10.1016/j.jqsrt.2012.04.022

Results were presented in these conferences:

[K1] A. Abola, A. Rimsa, Z. Brike, R. Veilande, G. Revalde. Zeeman AAS – a means to assess mercury pollution in the environment through artefacts of wild birds. XXXVth International Conference on Phenomena in Ionized Gases, Egmond aan Zee, Netherlands, July 9 – 14 (2023), p. 259

[K2] A. Abola, G. Revalde. Self-modulation in arsenic high-frequency electrodeless lamps. XXXVth International Conference on Phenomena in Ionized Gases, Egmond aan Zee, Netherlands, July 9 – 14 (2023), p. 295

[K3] G. Revalde, A. Abola, N.Zorina, A.Skudra. Investigation of radiation of Hg 198 isotope lamp. XXXVth International Conference on Phenomena in Ionized Gases, Egmond aan Zee, Netherlands, July 9 – 14 (2023), p. 246

[K4] A. Abola, Z. Brike, G. Revalde, R. Veilande, A. Rimsa, M. Strazds. Use of Zeeman AAS for mercury determination in black storks. European Winter Conference on Plasma Spectrochemistry, Ljubljana, Slovenia, January 29th – February 3rd (2023), p. 203

[K5] A. Abola, G. Revalde, A. Skudra, N. Zorina. Stability of low temperature plasma radiation in high frequency electrodeless light sources. European Winter Conference on Plasma Spectrochemistry, Ljubljana, Slovenia, January 29th – February 3rd (2023), p. 137

[K6] A. Ābola, M. Strazds, Z. Briķe, R. Veilande, K. Rancāne. Analysis of mercury concentration measurements in the faeces of black storks. 15th International Conference on Mercury as a Global Pollutant, virtual, July 24 – 29 (2022), ID59

[K7] G. Rēvalde, A. Ābola, N. Denisova, R. Veilande. The Role of the Operating Position of Mercury Capillary Light Sources. 14th European Conference on Atoms Molecules and Photons, Vilnius, Lithuania, June 27th – July 1st (2022), p. 280

[K8] K. Rancāne, A. Ābola, G. Rēvalde. Spectral measurements of mercury containing high frequency electrodeless lamps. 18th International Young Scientist Conference Developments in Optics and Communications 2022, virtual (Riga, Latvia) April 21–22 (2022), p.51

[K9] K. Rancāne, A. Ābola. A Comparison of the spectral properties in the UV region of arsenic high frequency electrodeless lamps and hollow cathode lamps. 65th International Conference for Students of Physics and Natural

Sciences Open Readings 2022, virtual (Vilnius, Lithuania), March 15 – 18 (2022), p. 194

[K10] Z. Brike, R. Veilande, M. Strazds, K. Rancane, A. Abola, A. Skudra. Mercury concentration in the faeces of black storks. 22nd International Scientific Conference EcoBalt2021, Riga, Latvia, October 21–23(2021), p.35

[K11] A. Abola, E. Bogans, A. Skudra, Z. Gavare, M. Strazds. Survey of total mercury concentration levels in eggshells of black storks. 14th International Conference on Mercury as a Global Pollutant, Krakow, Poland, September 8 – 13 (2019), p. 232

[K12] A. Skudra, N. Zorina, A. Abola, G. Revalde. Study of As spectrallines for discharge diagnostic purpose. 46th EPS Conference on Plasma Physics, Milan, Italy, July 8 – 12 (2019), P5.3002.

[K13] A. Ābola, Z. Gavare, E. Bogans, M. Strazds. Determination of total Mercury concentration in eggshells of Black Storks. International Conference Ecobalt 2018, Vilnius, Lithuania, October 25 – 27 (2018) p. 36

[K14] A. Ābola. Spectral comparison of As and Hg containing high frequency electrodeless lamps and hollow cathode lamps. 14th International Young Scientist conference Developments in Optics and Communications 2018, Riga, Latvia, April 12–13 (2018), p.46.

[K15] A. Ābola, Z. Gavare, E. Bogans, M. Strazds. Studies of mercury levels in black storks and their habitat. 19th International Scientific Conference Ecobalt 2014, Riga, Latvia, October 8 – 10 (2014) p. 10

[K16] A. Svagere, Z. Gavare, J. Skudra, M. Zinge. Intensity changes in time of high–frequency electrodeless discharge lamps containing heavy metals. 5th International Workshop on Plasma Spectroscopy, Giens, France, May 13 – 16 (2012), p. 42

[K17] Z. Gavare, A. Svagere, J. Skudra, V. Fyodorov. Studies of self–modulation phenomena in high–frequency electrodeless lamps. In abstracts of 5th International Workshop on Plasma Spectroscopy, Giens, France, May 13 – 16 (2012), p. 31

[K18] A. Švāgere, J. Skudra. Intensity stability measurements of high–frequency electrodeless discharge lamps. 55th scientific conference for young students of physics and natural sciences Open Readings 2012, Vilnius, Lithuania, March 28 – 31 (2012), p. 49

1. Theoretical background

1.1. Atomic absorption spectroscopy

Atomic absorption spectroscopy (AAS) is one of the first commercially developed analytical methods for the determination of concentrations of chemical elements. The operation of an atomic absorption spectrometer is based on Lambert–Beer's law of light absorption.

1.1.1. Basic principles of AAS

When a parallelly oriented flow of radiation with an intensity I_0 goes through a cell with a length of x (figure 1.1), which contains atoms of the element to be determined, the intensity of the transmitted radiation I_ν is described as [30]:

$$I_\nu = I_0 e^{-K_\nu x}, \tag{1.1}$$

where I_0 is the intensity of incident light, I_ν is the intensity of transmitted light, x is the length of the cell, K_ν is the absorption coefficient of the medium.

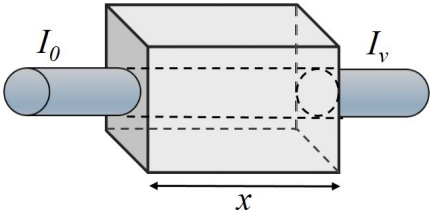

Figure 1.1: **Atomic absorption cell with a length of x. I_0 is the intensity of incident light, I is the intensity of transmitted light. The cell contains an element with a concentration of C.**

Using changes in radiation intensity I, it is possible to calculate the concentration of the element in the cell with the help of the Lambert–Beer law [30]:

$$log(\frac{I_0}{I}) = A = K_\nu x C, \tag{1.2}$$

where A is absorbance, K_ν is the absorption coefficient (constant in the given system), x is the length of the cell, C is the concentration of an element in the cell.

The expression 1.2 assumes that absorbance and concentration are linearly related provided that K_ν and x remain constant. Therefore, it is important to note that the half–width of the spectral line used for measurements must be narrower than the half–width of the absorption profile. Otherwise, concentration and absorbance will no longer have a linear relationship, since the absorption coefficient K_{nu} value will depend on the frequency [30]. During measurements, the system is always calibrated using an appropriate certified reference material. With its help, the relationship between concentration and change of intensity is

determined for the current conditions.

1.1.2. Light sources for atomic absorption spectroscopy

In atomic absorption spectroscopy, mainly line spectra light sources are used. For a line spectrum light source to meet the requirements necessary for AAS, it requires certain properties [13, 31]:

1) narrow and intense spectral lines;
2) resonance lines have little reabsorption and are not self–reversed;
3) the necessary spectral lines do not overlap with other spectral lines, as well as, in their vicinity, there are no other, disturbing, spectral lines;
4) the radiation must be stable over time;
5) it is desirable that the light source would be mechanically durable, quickly transferred into optimal working conditions, and with a long lifetime.

In addition to these conditions, it is useful if the light source and the elements required for its operation are small in size and light in weight, as it allows to manufacture small and portable devices [13, 32].

Currently, three types of light sources fit this description the best – hollow cathode lamps (HCLs), high–frequency electrodeless lamps (HFEDLs), and lasers. The choice of the light source is influenced by the chosen element and the objectives of the work.

1.2. Radiation and its characteristics

The intensity of the emission spectral line is determined by the concentration of atoms at excited level i and transition probability to a lower energy level k, and it is described by Einstein's equation [9]:

$$I_{ik} = A_{ik} N_{ik} h\nu_{ik} = A_{ik} N_k N_i h\nu_{ik} \int_0^\infty v(\nu)\sigma_{ki}(\nu)\nu^2 d\nu, \qquad (1.3)$$

where N_i – concentration of atoms in excited state i, A_{ik} transition probability from level i to k, N_k – concentration of atoms in ground state k, h – Planck's constant, ν_{ik} – frequency of transition, σ_{ki} – excitation cross section, $v(\nu)$ – function of electron velocity distribution.

1.2.1. Spectral line profiles

Spectral line profiles are important sources of information for plasma diagnostics because their form is influenced by various processes happening in the plasma [33]. As a result of these processes, spectral line broadening occurs. In high–frequency electrodeless lamps dominant are Doppler and Lorentz broadenings [34].

Instrument function

The shape of the line contour is also influenced by the hardware (spectrometer) used to record the spectra, the effect of which is described by the instrument function.

In high–temperature and dense plasmas, the width of the instrument function is much smaller than the width of the spectral lines, so it can be neglected. On the other hand, in low–temperature plasmas such as those found in HFEDLs, the width of the instrument function is comparable to the width of the experimental line profile, so to estimate the true shape and width of the line, it is necessary to separate it from the instrument function [35].

The measured spectral line profile $f(x)$ is a convolution of instrument function $f'(x)$ and real spectral line contour $f''(x)$, and it can be described as follows [33]:

$$f(x) = \int_{-\infty}^{+\infty} f''(x-y)f'(y)dy + \zeta(x), \tag{1.4}$$

where $\zeta(x)$ – function, describing random errors.

To find the real contour of spectral line $f''(x)$, it is necessary to solve the inverse task. Finding a solution of inverse task, by using Tikhonov's method is described, for example, in [35] and [36]. By using Tikhonov's regularization algorithm, the initial equation 1.4 is transformed into a functional minimization task. In such cases calculation of the real profile involves the search for minimum value for the following functional [35]:

$$M_\alpha[y, \tilde{f}] = \left\| \tilde{A}y - \tilde{f} \right\|_F^2 + \alpha\Omega[y], \tag{1.5}$$

kur $\alpha > 0$ regularization parameter, $\left\| \tilde{A}y - \tilde{f} \right\|_F^2$ – discrepancy, Ω – stabilizing functional.

1.2.2. Self–absorption

The form of spectral lines is important because with the increase in the line width, the absorption cross–section changes, and consequently, also changes the sensitivity of atomic absorption method.

In low–pressure plasma, one of the main factors influencing line shape is self–absorption, which results in the broadening of the lines [34].

Before resonant radiation can escape from the light source, it must first pass through the source. During this passage, there is a chance that atoms in the ground state will absorb the radiation, diminishing the released radiation. The self–absorption process is highly dependent on the distribution of metal atoms in the ground and excited states [9]. It affects the line shape, broadening, and intensity.

Self–absorption can be characterized by the coefficient I_{max}/I_0, expressed as the ratio of the maximum intensity of the spectral line I_{max} to the intensity at the center of the spectral line I_0. Schematically, the respective intensities in the spectral line contour are marked in figure 1.2

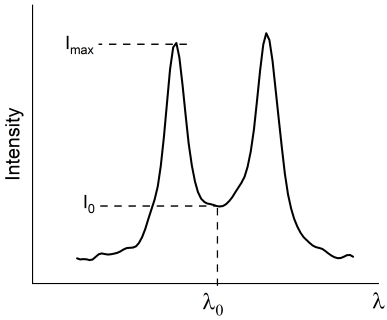

Figure 1.2: **An example of self–absorbed spectral line. Intensity values I_{max} and I_0 for calculation of self–absorption coefficient I_{max}/I_0 are marked on the contour.**

1.2.3. Determination of plasma temperature, using Boltzmann distribution over rotational levels

An important parameter in plasma diagnostics and practical applications is its temperature [37]. Various temperatures are distinguished to describe the processes occurring in plasma, including kinetic temperatures (of electrons, ions, and atoms), excitation temperature, ionization temperature, and rotational temperature [38]. The kinetic temperature of atoms is often referred to as the gas temperature, and it is assumed to be equal to the rotational temperature [37].

A popular method for determining temperature in plasmas is the use of single–element rotational or vibrational level series that follow the Boltzmann distribution [37, 39]. In such cases, several conditions must be met: the plasma must be in local thermodynamic equilibrium, the spectral lines used must be optically narrow, and they must not be self–absorbed [40].

This method can be used to determine the temperature, for example, from the OH radical's Meinel transitions ($A^2\Sigma^+ \rightarrow X^2\Pi; \nu' = \nu'' = 0$) – rotational bands at 306.4 nm. It has been found that OH radicals are formed in plasma even at very low concentrations of hydrogen [39]. In light sources such as HFEDLs, the formation of OH radicals is related to the presence of oxygen and hydrogen in the quartz composition of the lamp wall, which is introduced during the manufacturing process [41].

In the case of OH radical, rotational temperature can be determined, using the following expression [38, 42]:

$$lg\left(\frac{I_{ik}\lambda_{ik}}{A_{ik}}\right) = lg(C) - \frac{0,625E_{rot}}{T^{rot}}, \tag{1.6}$$

where λ_{ik} – spectral line wavelength, I_{ik} – spectral line intensity, A_{ik} – transition probability, E_{rot} – upper level energy [cm^{-1}], T^{rot} – temperature, C – constant. $\frac{I_{ik}\lambda_{ik}}{A_{ik}}$ is called reduced intensity. Its logarithm can be graphically plotted in dependence of energy E_{rot}, in the result obtaining points, that, in the case of Boltzmann distribution, can be linearly approximated. Then from the slope of

the approximation line, the temperature T^{rot} can be calculated.

The molecular band of OH radical ($A^2\Sigma^+ \rightarrow X^2\Pi$) at 306,4 nm with partially deciphered spectral lines of P, Q and R branches is shown in figure 1.3.

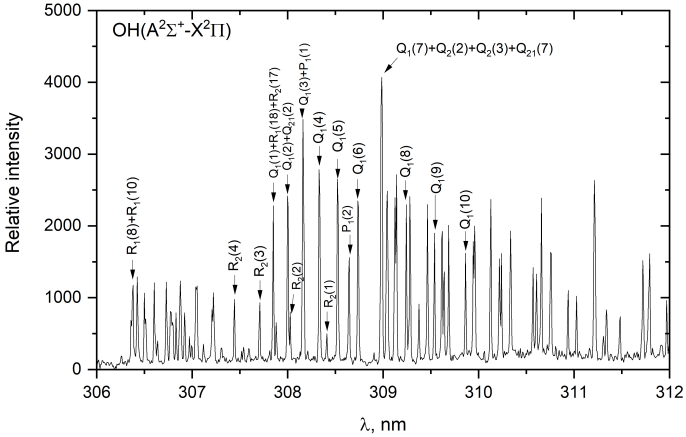

Figure 1.3: **OH radical ($A^2\Sigma^+ \rightarrow X^2\Pi$) spectral band at 306,4 nm (adapted from P11).**

Data necessary for temperature calculations from the OH radical (A–X) rotational band (0–0) Q_1 branch are given in table 1.1.

Table 1.1:
Spectral line transition parameters for temperature determination of OH radical (A–X) rotational band (0–0) [43, 44].

Spectral line	λ, nm	E, cm^{-1}	A, 10^8 s^{-1}
$Q_1(4)$	308,328	32779	33,7
$Q_1(5)$	308,517	32948	42,2
$Q_1(6)$	308,734	33150	50,6
$Q_1(8)$	309,239	33652	67,5
$Q_1(9)$	309,534	33952	75,8
$Q_1(10)$	309,859	34283	84,1

1.3. High–frequency electrodeless discharge – types and excitation

1.3.1. Excitation of electrodeless discharge

The excitation of an electrodeless discharge occurs with the help of external electrodes. Depending on the excitation scheme, either inductively or capacitively coupled discharge can be obtained [34]. High–frequency electrodeless discharge is generated by exciting it with a frequency ranging from 24 to 2450 MHz [13]. To initiate the excitation, the light source is placed in a high–frequency generator coil, which generates a changing electromagnetic field. When the electric field in the gas exceeds a certain value, electrons acquire enough energy to

ionize and excite atoms. As a result, discharge in the lamp begins. Initially, the excitation occurs, and the discharge is observed in the inert gas.

The plasma in high–frequency capacitive lamps is of low temperature, partially ionized, and in local thermodynamic equilibrium.

1.3.2. Types of electrodeless discharge

There are at least two types of electrodeless discharge: E–discharge, also called preliminary discharge and H–discharge or curling discharge. E–discharge is excited by electric field by potential field intensity $\vec{E}_p = -grad\varphi$, meanwhile H–discharge excites in a magnetic field by electric curling field with intensity $\vec{E}_v = -\frac{\delta \vec{A}}{\delta t}$ [31, 45]. In a real discharge both types co–exist, and the resulting electric field is described by

$$\vec{E} = -grad\varphi - \frac{\delta \vec{A}}{\delta t}, \tag{1.7}$$

where $\vec{A}$ – field's vector potential, φ – scalar potential. Usually $|grad\varphi| > \left|\frac{\delta \vec{A}}{\delta t}\right|$, and because of that E–discharge is ignited first, but, when increasing the electron concentration (up to $3 \cdot 10^{10}$ cm^{-3}), ignition of H–discharge is observed [45].

1.3.3. Self–modulation

In some light sources, due to the processes occurring in them, as the applied excitation generator power increases, the radiation transitions into a self–modulation regime – its intensity periodically fluctuates by increasing and decreasing. The self–modulation process can be divided into two phases – the maximum phase and the minimum phase.

During the maximum phase, the light source is bright and high–intensity curling discharge occurs. The end of this phase is marked by a rapid drop in intensity, which can be explained by changes in the energy of free electrons. As the gas temperature increases, the vapor pressure of the elements in the lamp increases. Consequently, electron collisions with element atoms occur more frequently until, at some point, the electrons can no longer accumulate enough energy to continue excitation and jonization processes. This leads to a decrease in the intensity of radiation emission, and the minimum phase begins [45, 46].

The minimum phase is characterized by low–intensity emission from the working element and buffer gas. One of the theories suggests that during this phase, the radiation transitions into the E–discharge [45]. As the plasma cools down, the concentration of particles in the lamp's volume decreases. Consequently, electrons interact less with them and can gain enough acceleration to restart the excitation process. A gradual transition into the maximum phase is observed.

Intensity fluctuations during self–modulation are periodic, so it is possible

to calculate its period T:

$$T = \frac{t}{n}, \tag{1.8}$$

where n is the number of full self–modulation cycles during the measurement period and t is the time to complete these full cycles.

In the thesis self–modulation is studied in As HFEDLs, but it can be also observed in HFEDLs with such fillings as TlI_2 [41], BiI_3 [46] and [K17], $SnCl_2$ [K17], Se [K18].

2. Equipment and light sources

2.1. Investigated light sources

The study focused on spherical–shaped HFEDLs containing arsenic. These lamps are made of quartz glass, with a spherical part diameter of 10 mm (figure 2.1 a)). They have a small, few millimeters long capillary. The working element is arsenic, and the buffer gas is argon with a pressure of approximately 3 torr. To initiate radiation, the lamps are placed in a coil, and excitation occurs in the lamp's bulb.

As lamps can be manufactured with or without a getter. A getter is a material introduced into the lamp to capture various unwanted impurities present in it that may arise during the lamp's manufacturing process. One of the purposes of introducing a getter is to improve the stability of lamp radiation [47].

The spectrum of the arsenic lamp in relative intensity units in the UV range from 180 nm to 300 nm is shown in figure 2.2. Three As resonance lines which are of interest for absorption studies are highlighted in the spectrum: 189.0 nm (transition $^4P_{5/2} \rightarrow {}^4S^o_{3/2}$), 193.8 nm (transition $^4P_{3/2} \rightarrow {}^4S^o_{3/2}$), and 197.3 nm (transition $^4P_{1/2} \rightarrow {}^4S^o_{3/2}$) [48].

The study considered two forms of mercury HFEDL. The spherical Hg lamp is similar to the As HFEDL described above. The capillary Hg lamp (figure 2.1 b)) is made of a cylindrical tube approximately 20 mm long with an internal diameter of 1 mm, with a spherical bulb with a diameter of 10 mm at one end. Argon or xenon gas at a pressure of approximately 2–3 torr was the buffer gas. In this case, the lamp is operated using externally connected capacitively coupled electrodes. The applied high–frequency electromagnetic field frequency is approximately 300 MHz, and the operating power is about 3 – 9 V. Excitation occurs in the capillary of the lamp.

The spectrum of the mercury HFEDL in relative intensity units in the 180 – 600 nm range is shown in figure 2.3. Atomic absorption spectrometry uses the Hg 253.7 nm resonance spectral line (transition $^3P^o_1 \rightarrow {}^1S_0$).

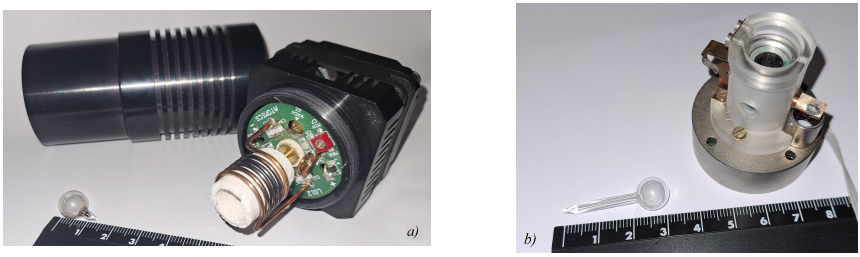

Figure 2.1: **Example of investigated light sources together with their excitation generators: a) arsenic lamp; b) mercury capillary lamp.**

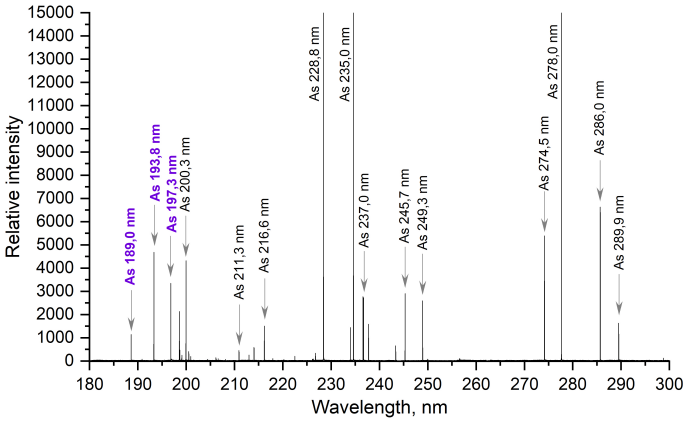

Figure 2.2: **UV spectrum of As HFEDL from 180 to 300 nm.**

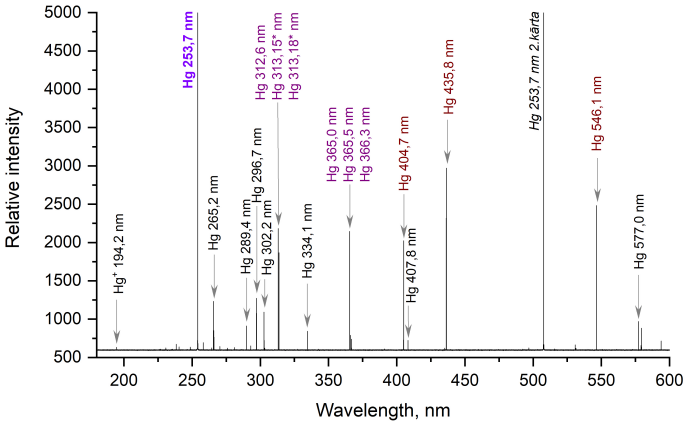

Figure 2.3: **Spectrum of Hg HFEDL from 180 to 600 nm.**

2.2. Spectrometers

Three spectrometers with different resolution capability were used to record spectral data:

1) *Avantes AVS-PC2000 „plug–in" type spectrometer.* Its spectral resolution is 0,36 nm, and it can simultaneously register spectrum in the range of 190 nm to 850 nm.
2) *Spectrometer Jobin Yvon SPEX 1000M.* Equipped with 1200 lines/mm diffraction grating, its focal length is 1 m, and spectra are registered with a thermoelectrically cooled CCD camera. The range for spectral registration is from 180 to 850 nm, spectral resolution is 0,008 nm.
3) *Fourier transform spectrometer Bruker IFS–125HR.* Its spectral resolution is 0,0015 cm^{-1} or $5{,}4 \cdot 10^{-5}$ nm.

2.3. Equipment for mercury concentration measurements

Mercury concentration measurements were conducted using the RA–915M atomic absorption analyzer, which employs the Zeeman effect for background correction. One of the main components of the instrument is a high–frequency electrodeless Hg capillary lamp filled with mercury isotope vapor (either ^{198}Hg or ^{204}Hg) and placed in a constant magnetic field.

To measure mercury concentrations in water, the analyzer was used in conjunction with the attachment RP–92, designed for cold vapor atomic absorption. In this case, the instrument's detection limit for Hg in water is 0.5 ng/l [49].

By using the RA–915M analyzer in combination with the pyrolytic furnace PIRO–915+, it is possible to perform mercury concentration measurements in various biological, natural, and food product samples. The advantage of this method lies in the simplicity of sample preparation, as there is no need to dissolve solid samples or prepare them chemically. Minimal sample pre–treatment reduces the risk of contaminating the samples and minimizes the loss of the analyte. In this setup, pyrolysis is used to convert all mercury species in the sample into atomic mercury. The detection limits for solid samples range from 0.5 to 5 ng/g (lower limit for soil, higher limit for organic materials) [49].

2.4. Water sample collection and preparation for measurements

Mercury concentration measurements in water samples were conducted as part of a collaborative interlaboratory study organized by Brook Rand Labs. Sample collection from three sampling sites in the state of Washington, USA (Heron Pond, Sunset Pond, Everett North), was facilitated by the study organizers. After collection, the samples were preserved using a hydrochloric acid solution to prevent the volatilization of mercury. To ensure uniformity of the samples, samples underwent homogenization, and meticulous checks were performed to guard against contamination during preparation [50]. After receiving the samples, the analysis was conducted within four weeks, and the results were reported.

Sample preparation involved the mineralization of samples, during which all mercury in the sample was converted into Hg^{2+} ions. The instrument was calibrated using the NIST SRM 3133 standard for mercury measurements in liquids. To perform the measurements, the mineralized sample was mixed with a reducing solution ($SnCl_2$ solution), converting Hg ions into elemental mercury, which was then directed into the analytical cell by airflow and detected by the analyzer.

2.5. Description of black stork samples and context for measurement necessity

The use of various natural samples in environmental monitoring is a widely employed method for assessing pollution in the environment [27]. In the case of birds, the presence of a selected toxic element can be analyzed in blood [51], feathers [51, 52], eggs [53, 54], and their inner membranes [54–56], [P1, P3, P4], and feces [P3, K10].

Researchers aim to employ non–invasive methods when possible, as obtaining such samples is simpler and less disruptive to birds [54, 56], [P1, P4]. Additionally, in the case of eggs, studying eggshells (either hatched or failed eggs) does not affect the number of viable young birds, which is particularly important for endangered species [P1]. Such species include the black stork (*Ciconia nigra*) in Latvia, as various factors such as logging, issues with finding food, and environmental pollution are reducing the number of successfully nesting pairs in Latvia [26].

Black Storks are fish–eating birds, with small freshwater fish making up the majority of their diet. As a result, they are exposed to a higher risk of mercury intake due to Hg accumulation in the food chain [29, 57].

In this study, mercury concentration measurements were conducted in black stork eggshells and feces, in collaboration with ornithologist Dr. Biol. Māris Strazds, who collected and marked the samples. The samples were collected from nesting sites all across Latvia.

After collection, eggshell samples were cleaned and dried under room conditions. Before measurements, membranes were separated from the eggshells, and both membranes and eggshells were crushed using a mortar and pestle. In cases where membranes could not be separated from eggshells, mixed samples were used.

Fecal samples were collected along with the vegetation on which they were found (branches, leaves, bark). Subsequently, they were labeled with the collection date and nest number. Before measurements, feces were separated from the vegetation as much as possible, and their visual appearance (color) was assessed.

Instrument preparation for measurements included calibration using an appropriate reference material. For eggshell measurements, the mussel tissue standard ERM–278k (*European Commission Joint Research Centre*) was used, while for fecal measurements, the standard BCR–060 (*Lagarosiphon major*, *European Commission Joint Research Centre*) was employed.

3. Spectral measurements of arsenic–containing high–frequency electrodeless lamps

Within the scope of this work, 20 high–frequency electrodeless lamps containing arsenic were examined. They can be divided into 2 groups: 16 lamps without a getter and 4 lamps with a getter placed in them. These lamps were manufactured at the Laboratory of High–Resolution Spectroscopy and Light Source Technology of the Institute of Atomic Physics and Spectroscopy. To identify each lamp, they were assigned numbers, that were also used to represent the results. Lamps with getters are denoted with "G" (G1, G2, G3, G4), while lamps without getters are denoted with "L" (L1, L2, L3, L4, L5, L8, L11, L13, L14, L15, L16, L17, L18, L19, L21, LK). All the studied As spectral lines and their characteristics are provided in table 3.1. Special attention was given to the resonance spectral lines with wavelengths of 189.0 nm, 193.8 nm, and 197.3 nm.

Table 3.1:
Wavelengths, levels, and transition probabilities of arsenic spectral lines, used in the work [48].

Wavelength λ, nm	Lower level	Upper level	Trans. probab. A_{ik}, 10^8 s^{-1}
189.0	$4s^2 4p^3\ [^4S^o_{3/2}]$	$4s^2 4p^2(^3P)5s\ [^4P_{5/2}]$	2.7
193.8	$4s^2 4p^3\ [^4S^o_{3/2}]$	$4s^2 4p^2(^3P)5s\ [^4P_{3/2}]$	2.2
197.3	$4s^2 4p^3\ [^4S^o_{3/2}]$	$4s^2 4p^2(^3P)5s\ [^4P_{1/2}]$	2.0
235.0	$4s^2 4p^3\ [^2D^o_{3/2}]$	$4s^2 4p^2(^3P)5s\ [^2P_{1/2}]$	3.1
245.7	$4s^2 4p^3\ [^2D^o_{5/2}]$	$4s^2 4p^2(^3P)5s\ [^4P_{3/2}]$	0.072
278.0	$4s^2 4p^3\ [^2P^o_{3/2}]$	$4s^2 4p^2(^3P)5s\ [^2P_{3/2}]$	0.78

The arsenic lamp spectra were studied with respect to:

1) their manufacturing type (with or without a getter);
2) excitation generator voltage or power;
3) the type of generator used.

Within the scope of this work, self–absorption, intensity, and radiation stability of As spectral lines were assessed, the self–modulation regime of As lamps was investigated, and the gas temperature within the lamps was evaluated.

3.1. Determining the effect of the getter on lamp spectra

The main purpose of the getter is to „collect" impurities that enter the lamp during the manufacturing process and which can affect the lamp's operation, and to achieve that spectrum is mostly made of arsenic and argon spectral lines. Various compounds containing hydrogen, oxygen, nitrogen, and carbon, such as OH^-, N_2, CO_2, CO, etc., can enter the lamps during the lamp manufacturing process.

An example of a spectrum where molecular bands are observed is shown

in figure 3.1 a), which displays the getterless lamp's spectrum in the range from 240 nm to 340 nm with clearly visible molecular bands in the 250 – 300 nm range, at 306 nm, and in the 310 – 335 nm range. The spectrum recorded for a lamp with a getter in the same conditions is shown in figure 3.1 b). Comparing both images, it is evident that the intensities of impurity molecule bands are several times lower in the presence of a getter. These changes demonstrate that the getter acts to significantly reduce the amount of unwanted impurities.

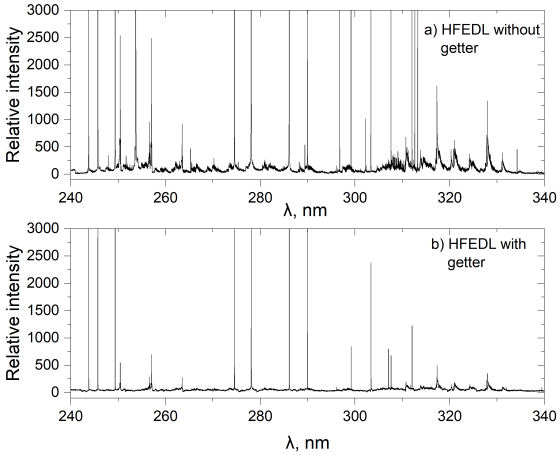

Figure 3.1: **Spectrum range of 240 nm to 340 nm for an As HFEDL a) lamp without getter; b) lamp with getter.**

3.2. Studies of As high–frequency electrodeless lamp spectral line intensities

The relative intensities of spectral lines were recorded using a Jobin Yvon spectrometer. The *Integrate* function of OriginPro 2019b software was used to obtain integral intensities. Each spectral line at each power value was recorded five times, and then the average value was calculated. Standard deviation was used to characterize the differences in spectral line intensities. The error values obtained depended on the spectral line intensity – for lower intensities they were larger; however, overall, relative errors did not exceed 5%.

3.2.1. Relative intensities of arsenic resonance spectral lines

One of the important steps in evaluating lamp performance is determining changes in spectral line intensities depending on the excitation generator power (or voltage, current). Figure 3.2 shows the intensity changes as a function of excitation generator power in the range of 12 to 22 W for three As resonance lines, 189.0 nm, 193.8 nm, and 197.3 nm, in 7 As HFEDLs without a getter. The remaining 9 out of the 16 examined lamps exhibited self–modulation at relatively low generator power levels (see Section 1.3.3), so they were not included in these graphs.

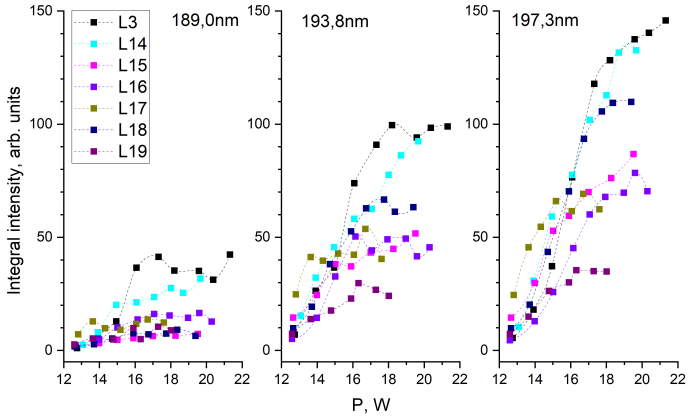

Figure 3.2: **The change of relative intensities in dependence of excitation generator power in the 12 – 22 W range for arsenic resonance spectral lines with wavelengths 189.0 nm, 193.8 nm, and 197.3 nm in HFEDLs without a getter.** Remark: experimentally obtained points are connected for better visuality only.

Theoretically, it is expected (see table 3.1) that the 189.0 nm spectral line will be the most intense, while the intensity of the 197.3 nm spectral line will be the lowest. However, figure 3.2, shows that the measured intensities of the 189.0 nm spectral line are several times lower than those of the 193.8 nm and 197.3 nm spectral lines. Similarly, it can be observed that the intensity of the 197.3 nm line is higher than that of the 193.7 nm line. These differences are related to two factors – firstly, the sensitivity of the spectrometer rapidly changes in the 180 nm – 200 nm range, and at 189 nm, it is lower. Secondly, in the 180 nm – 200 nm range, the oxygen absorption capacity in the air increases significantly. Due to the relatively long distance the radiation has to travel in the air from the light source to the spectrometer matrix (2 m), atmospheric oxygen can partially absorb this radiation. For these reasons, the observed intensity of the 189.0 nm spectral line is lower than that of the other two resonance lines.

When using HFEDLs in atomic absorption spectrometers, the distance the radiation has to travel is shorter, but atmospheric oxygen can still partially absorb it. This should be taken into account when choosing the most suitable spectral line for absorption measurements.

Comparing data from several HFEDLs, it is observed that the radiation intensity varies slightly between lamps. Lamps L3 and L14 exhibit higher relative intensities for spectral lines than the others. Differences between lamps can be explained by factors such as the lamp manufacturing process and operating conditions. Although lamps are usually manufactured in small groups, each lamp is considered an individual, as some manufacturing steps, such as melting and post–melting processing, are performed separately for each lamp. On the other hand, operating conditions are influenced by the environment, such as tempera-

ture, and the lamp's placement in the excitation generator socket. To better compare lamps with each other, the same measuring conditions are chosen, but some deviations are possible. Additionally, it is evident that there are common trends observed in the group of lamps – the previously described spectral line ratio is maintained in all lamps, and spectral line intensities are within reasonably similar values. All lamps exhibit the expected increase in spectral line intensity as the excitation generator power is augmented. At higher power levels, it can be seen that the radiation starts to saturate, and the intensity does not further increase. One possible explanation for this is the self–absorption of these spectral lines.

Out of the studied 20 As HFEDLs, four had getters. The changes in the intensities of the As resonance lines 189.0 nm, 193.8 nm, and 197.3 nm as a function of excitation generator power in the 11 to 22 W range for these lamps are shown in figure 3.3.

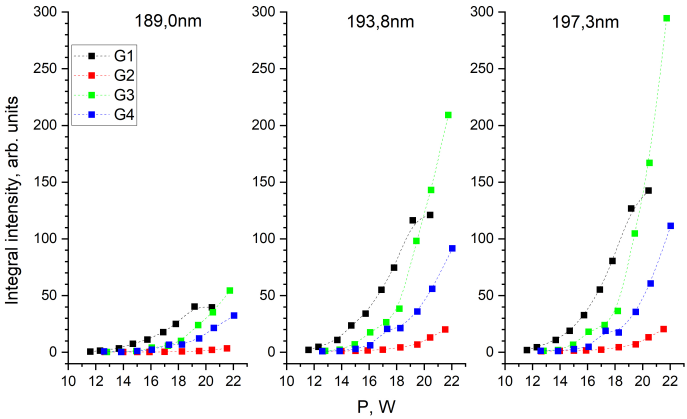

Figure 3.3: **The change of relative intensities in dependence on excitation generator power in the 11 – 22 W range for arsenic resonance spectral lines with wavelengths 189.0 nm. 193.8 nm and 197.3 nm in HFEDLs with a getter.** Remark: experimentally obtained points are connected for better visuality only.

For lamps with getter, it is also observed that the 189.0 nm spectral line has the lowest recorded intensity, while the 197.3 nm spectral line has the highest intensity. The intensity of spectral lines at lower excitation generator powers is similar in all four lamps but, as the power increases, the intensities in the lamps increase at different rates. The lowest relative intensity values were observed in lamp G2, while the highest were in lamp G3.

Comparing lamps with a getter to the getterless ones, it is evident that the relative intensity for lamps G1 and G4 is similar to what is recorded in getterless lamps. The intensity of spectral lines in lamp G3 is higher, but in lamp G2, it is slightly lower than in lamps without a getter. Unlike lamps without a getter, lamps with a getter exhibit a rapid increase in intensity as the excitation generator power increases. In the given power range, radiation saturation is not observed.

This could be explained by the getter's ability to capture atoms and molecules that could potentially reduce emission radiation intensity. It can be concluded that the addition of getters improves the spectral properties of lamps.

3.2.2. Influence of the excitation generator on spectral line intensity

Certain As lamps were studied using two generators: one with an excitation frequency of 300 MHz (operating voltage range of 9 – 15 V) and another with a frequency of 100 MHz (operating voltage range of 20 – 29 V). The 100 MHz frequency excitation generator was operated at 20 – 29 V, which corresponded to approximately 11.5 – 20.5 W of power depending on the lamp's input current. The 300 MHz frequency excitation generator was operated at 9 – 15 V, which corresponded to approximately 4.0 – 12.0 W of power. The selected operating voltage was related to the processes occurring within the lamps and was chosen to be within a range where the recorded As spectral line radiation was sufficiently intense and stable.

The obtained relative intensity values for arsenic 189.0 nm, 193.8 nm, and 197.3 nm spectral lines as a function of excitation generator power for the lamp without a getter are shown in figure 3.4, while for a lamp with a getter, they are shown in figure 3.5.

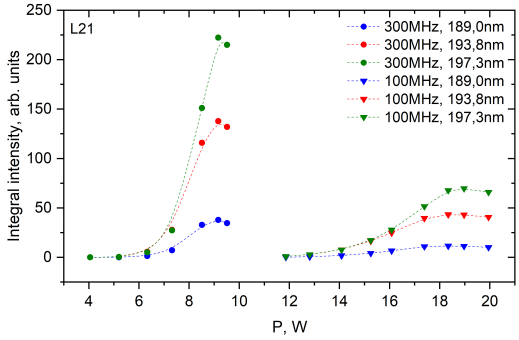

Figure 3.4: **Comparison of spectral line 189.0 nm, 193.8 nm, and 197.3 nm intensities in dependence of power of excitation generator, when using generators with 300 MHz (left) and 100 MHz (right) excitation frequency for lamp without getter.** Remark: experimentally obtained points are connected for better visuality only.

For both lamps using the 300 MHz frequency excitation generator, the emission of As resonance lines is more intense compared to using the 100 MHz frequency excitation generator. In the case of the lamp without a getter, the maximum relative intensity recorded with the 300 MHz frequency excitation generator is approximately 3 times higher than that with the 100 MHz frequency excitation generator for all three spectral lines. For the lamp with a getter, the intensity ratio is lower – the relative intensities for the 189.0 nm spectral line are similar, but for the 193.8 nm and 197.3 nm lines, the maximum intensity differs by approximately 2 – 2.5 times.

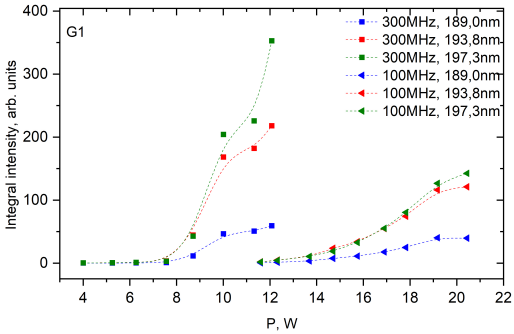

Figure 3.5: **Comparison of spectral line 189.0 nm, 193.8 nm, and 197.3 nm intensities in dependence of power of excitation generator, when using generators with 300 MHz (left) and 100 MHz (right) excitation frequency for lamp with getter.** Remark: experimentally obtained points are connected for better visuality only.

In any case, it is evident that the high–frequency electrodeless lamp with a getter has higher spectral line intensities. Additionally, when using the 300 MHz frequency generator, lower operating power is required to achieve high intensities – this can be achieved at around 10 – 12 W of power for the lamp with a getter and 8 – 10 W of power for the lamp without a getter. When operated at lower power, the lamp's lifetime is extended [9], making a higher–frequency generator potentially more suitable for lamp excitation for AAS applications.

3.3. Self–absorption

One of the main requirements for the use of HFEDLs in AAS is to minimize self–absorption of the used spectral lines because it reduces line intensity and broadens them.

To determine the impact of self–absorption, As spectral lines were measured using a high–resolution Fourier–transform spectrometer [P2, P5]. However, even in this case, to obtain real line profiles and assess the presence of self–absorption, it is necessary to remove the instrument function from the experimentally obtained spectrum.

Hereafter, the self–absorption of As resonance spectral lines in two arsenic lamps is examined. In the first lamp, more attention is paid to the 197.3 nm spectral line [P5].

In figure 3.6 a), the contour of the As 197.3 nm spectral line is shown before and after the removal of the spectrometer's instrumental function at 9.8 W generator power. It can be observed that although the instrumental function only slightly affects the line width, it „masks" the depth of the line self–absorption.

Figure 3.6 b) compiles the contours of the 197.3 nm spectral line at various excitation generator power values ranging from 5.2 W to 9.8 W. At 5.2 W, the line is not self–absorbed, but as the power increases, it becomes self–absorbed, and the dip at the line center deepens, while the line width also increases.

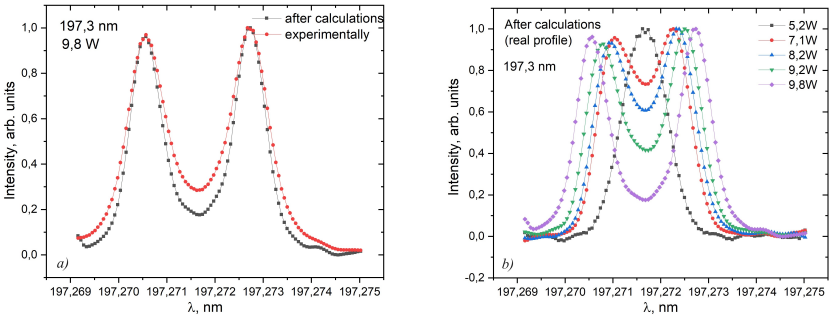

Figure 3.6: **Profile of As 197.3 nm spectral line and its changes: a) experimentally obtained profile and profile after deconvolution, b) profile changes in dependence on generator power in 5.2 – 9.8 W range after deconvolution [P5].** Remark: experimentally obtained points are connected for better visuality only.

In figure 3.7, the change in the self–absorption coefficient I_{max}/I_0 (see section 1.2.2) is shown as a function of the excitation generator power. The self–absorption coefficient is determined for both the experimentally recorded spectral line and spectral line after removing the spectrometer's instrumental function.

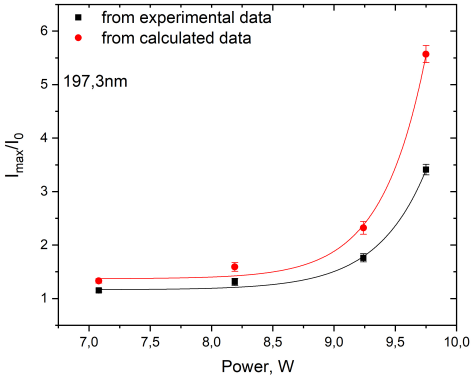

Figure 3.7: **Changes of self–absorption coefficient I_{max}/I_0 in dependence of excitation generator power before and after the removal of the instrument function for As 197.3 nm spectral line [P5].**

It can be concluded that the value of the self–absorption coefficient increases exponentially as the excitation generator power increases. Based on these data, the optimal operating power for this lamp is approximately 9 W. When comparing the values of the self–absorption coefficient for a spectral line before and after the removal of the instrument function, it can be observed that at higher excitation generator power, the coefficients differ more significantly. The instrument function has a greater impact on the real line profile and masks the self–absorption.

Similar processes were observed in the second examined HFEDL. In figure 3.8 a), the contour of the As 189.0 nm spectral line is shown before and after the removal of the instrument function at 15.1 W generator power. For this line as well, the instrument function masks the self–absorption dip.

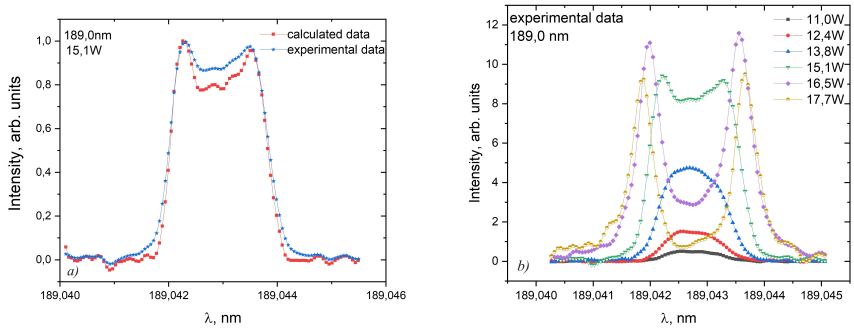

Figure 3.8: **Contour of As 189.0 nm spectral line and its changes: a) contour before and after removal of instrumental function. b) changes of contour depending on generator power in 11.0 to 17.7 W range. experimental data [P2].** Remark: experimentally obtained points are connected for better visuality only.

In figure 3.8 b), the contours of the As 189.0 nm spectral line are compared at generator powers ranging from 11.0 to 17.7 W before removing the instrument function. The intensity of the spectral line increases up to power values of 13.8 W, and at 15.1 W, the intensity is even higher, but a noticeable self–absorption dip becomes apparent at 16.5 W and 17.7 W.

For three arsenic resonance spectral lines their self–absorption was quantitatively assessed, using coefficient I_{max}/I_0, its values for six generator power values are given in table 3.2.

Table 3.2:

Self–absorption coefficient for As 189.0 nm. 193.8 nm and 197.3 nm spectral lines after removal of instrumental function. at various generator power values [P2].

	I_{max}/I_0					
Power. W	11.0	12.4	13.8	15.1	16.5	17.7
189.0 nm	1.0	1.0	1.0	1.2	5.4	31.0
193.8 nm	1.0	1.0	1.0	1.5	7.2	38.6
197.3 nm	1.0	1.0	1.0	1.1	2.8	8.9

As expected, the least self–absorption is observed for the 197.3 nm spectral line, since this line has the lowest transition probability among the examined As resonance lines (table 3.1).

Based on the transition probability values, the 189.0 nm spectral line would be expected to be the most self–absorbed. However, it was not confirmed in this study. Considering that the intensity of the 189.0 nm spectral line is most affected by the oxygen absorption capacity in the air, it is possible that the loss of intensity also influenced the self–absorption. It would be useful to perform spectral registration in a non–oxygen environment for wavelengths shorter than 190 nm.

When increasing the power, an increase in spectral line intensity is expected,

at the same time at higher powers self–absorption is observed. So it can be concluded that the optimal operating power for these lamps, based on these parameters, is approximately 14 – 15 W.

3.4. Radiation stability

Radiation stability is one of the key parameters characterizing the suitability of light sources for AAS. Lamp stability is described by several parameters, including radiation stabilization after switching on, stability during measurements (short–term stability – minutes, hours), long–term stability (lamp lifetime), and unstable operating modes (self–modulation).

To characterize lamp radiation stability over a longer period, comparable to the duration of AAS measurements, a stability graph of As resonance lines was recorded using a Jobin Yvon spectrometer. The total spectrum acquisition time was one hour, and spectra were recorded every 15 seconds. The results of the changes in the integral intensities of the 189.0 nm, 193.8 nm, and 197.3 nm spectral lines over an hour are shown in figure 3.9.

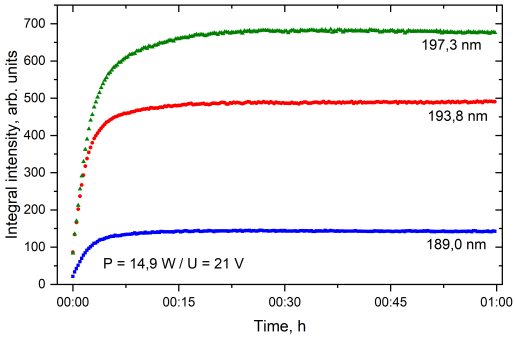

Figure 3.9: **Stability of As 189.0 nm, 193.8 nm and 197.3 nm spectral lines during 1 hour [P2, K5].**

After switching on, the lamp takes about 15 minutes to warm up. During this time, the radiation intensity increases rapidly and then begins to saturate.

Once the radiation stabilized, the integral intensity of the 189.0 nm spectral line fluctuated around the average value of 148 $\pm$ 1 relative units. The integral intensity of the 193.8 nm spectral line fluctuated around the average value of 491 $\pm$ 2 relative units. The integral intensity of the 197.3 nm spectral line fluctuated around the average value of 684 $\pm$ 2 relative units. The percentage radiation fluctuations were 0.7% for the 189.0 nm line, 0.4% for the 193.8 nm line, and 0.3% for the 197.3 nm line. Literature indicates that stable HFEDL radiation fluctuations do not exceed 2% [13], therefore it can be concluded that the examined As lamp operates stably.

To compare both the As and Ar spectral line changes over time, they need to be recorded simultaneously. The Avantes spectrometer provides this capability for the spectral range from 180 nm to 850 nm. Due to the limited sensitivity of the spectrometer, there is very low intensity for spectral lines at wavelengths shorter

than 200 nm. Therefore, other As spectral lines – 245.7 nm and 278.0 nm – were chosen to represent the processes occurring in the lamp. The stabilization of the 245.7 nm and 278.0 nm As lines, as well as the 763.5 nm and 811.5 nm Ar lines, over 20 minutes after setting the excitation generator voltage to 23 V, 25 V, 27 V, and 29 V, is shown in figure 3.10 [K18].

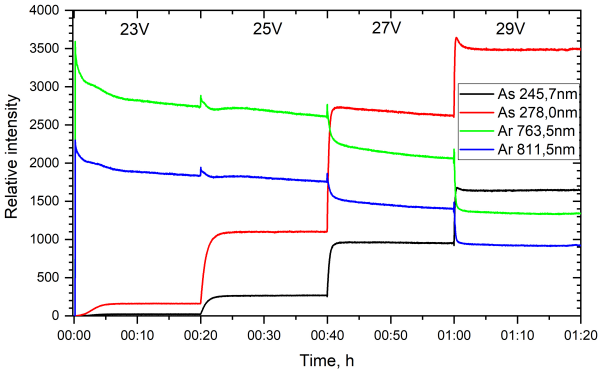

Figure 3.10: **Intensity changes of As 245.7 nm, As 278.0 nm, Ar 763.5 nm and Ar 811.5 nm spectral lines during 20 min after setting excitation generator voltage to values of 23 V, 25 V, 27 V un 29 V [K18].**

Immediately after setting the generator voltage, a rapid intensity change is observed, followed by radiation stabilization. Initial stabilization or warming up occurs in about 5 to 15 minutes, after which lamp is ready for operation. At the beginning of the discharge, there are only buffer gas atoms in the lamp, so the Ar spectral lines are more intense. As the lamp warms up, the pressure of As vapor increases, and consequently, the As discharge intensity increases. Increasing the excitation generator voltage results in a decrease in the Ar discharge – As line intensity increases, but the Ar line intensity decreases [K18].

3.5. Self–modulation

The stability of As HFEDLs was assessed at various voltage values of the excitation generator in the range from 20 to 29 V. Some of the As–containing HFEDLs switched to self–modulation mode at some point. The self–modulation spectra were recorded using a Jobin Yvon spectrometer.

3.5.1. Self–modulation depending on the lamp type

The lamps with a getter operated stably within the considered voltage range. This suggests that the presence of a getter helps to stabilize the operation of the lamps. Lamps without a getter could be divided into two groups: 1) some lamps operated stably up to a voltage of 27 – 28 V, and 2) for some lamps, self–modulation started at a voltage of 23 – 25 V. Due to the changing light intensity, atomic absorption measurements cannot be performed using light sources that operate in self–modulation mode. For this reason, for elements contained

in lamps where this effect is observed (including arsenic), to choose the optimal lamp operating mode, a) the power range in which the lamp operates stably must be taken into account, and/or b) changes in the lamp manufacturing technology must be introduced. However, although self–modulation has no direct application in atomic absorption spectroscopy, it can be used to study processes occurring in low–temperature plasmas and the interaction between atoms, ions, and molecules. Since the voltage remains constant during the self–modulation process, but the current changes, for the description of the self–modulation process the voltage of the excitation generator rather than the power was used.

3.5.2. Self–modulation of As and Ar spectral lines

It is known that excitation and discharge processes in the working substance and buffer gas vapors are interconnected. Initially, when buffer gas atoms are available in the lamp, the discharge starts in the buffer gas vapor first. However, as the lamp warms up and the metal in the lamp vaporizes, the excitation of the work element atoms becomes more active [34]. This gradual change in discharge can also be observed during self–modulation. Changes in the intensities of As 278.0 nm and Ar 763.5 nm spectral lines during self–modulation at 29 V in a lamp without a getter are shown in figure 3.11. It can be seen that in each cycle, the discharge first starts in argon. It is then followed by a gradual start of the discharge in As vapor and a simultaneous decrease in the intensity of Ar emission spectral lines. Then, the lamp overheats, and the intensities drop rapidly.

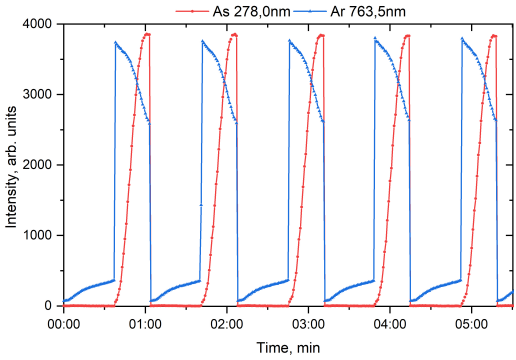

Figure 3.11: **Self–modulation of As 278,0 nm and Ar 763,5 nm spectral lines in As getterless lamp. Excitation generator voltage is 29 V [K2].**

3.5.3. Self–modulation at different voltage values

For the group of lamps without a getter, where self–modulation started at voltage values of 23 V to 26 V, the influence of the excitation generator voltage on the self–modulation regime was investigated.

For example, in figures 3.12 a) and b), self–modulation is observed for three As resonance spectral lines from the same As lamp at two different excitation generator voltages, namely 24 V and 28 V. From the graphs, it can be seen that

the formation of As vapor occurs more rapidly at 28 V, as the intensity of As spectral lines increases more quickly compared to the case with 24 V voltage. As the concentration of vaporized atoms and molecules reaches the point where there is no longer sufficient stimulation of radiation, the decrease in intensity also occurs earlier. Therefore, it is observed that increasing the voltage shortens the self–modulation period.

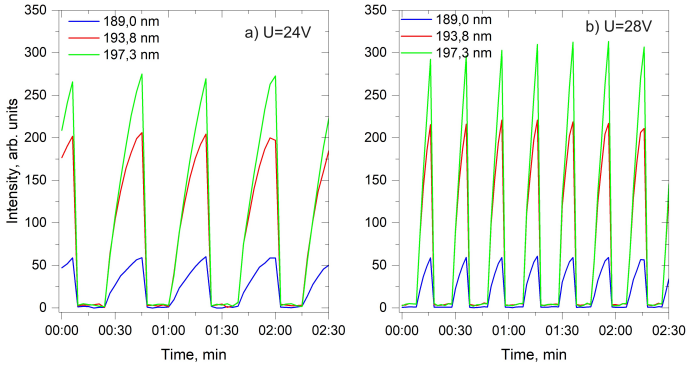

Figure 3.12: **Example of self–modulation for As 189.0 nm, 193.8 nm and 197.3 nm spectral lines at excitation generator voltage of a) 24 V, b) 28 V [K5].**

3.5.4. Determination of the self–modulation period

To calculate the period, self–modulation oscillations were recorded at excitation generator voltages ranging from 24 V to 29 V. At each of these generator voltage values, the self–modulation process was recorded for 2 to 3 minutes, during which 3 to 7 self–modulation cycles were repeated. These measurement cycles were repeated five times. The measurements were conducted under the same conditions, and the lamp was turned off and cooled between them to eliminate the influence of temperature.

Subsequently, using the expression 1.8, the self–modulation periods were calculated for each measurement cycle, and the average period values were calculated for each voltage value. The obtained average period values as a function of the generator voltage are shown in figure 3.13.

As the generator voltage is increased, the self–modulation period decreases because the processes in the lamp occur more rapidly. At 24 V, the average self–modulation period was 56 s, and it exponentially decreased further. At 29 V, the self–modulation period for HFEDL was 21 s. The largest difference between measurement cycles was observed at 24 V, with a relative error of approximately 17%. This difference may be explained by the fact that the voltage range between 23 V and 24 V for the lamp under study is a transition region between stable operation and self–modulation. Since self–modulation is related to physical quantities such as plasma temperature and the concentration of ions, atoms,

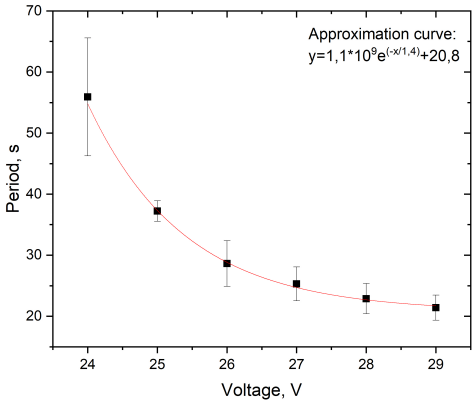

Figure 3.13: **Changes in self–modulation period in dependence on excitation generator voltage. Data points were approximated using exponent equation** $1.1 \cdot 10^9 e^{(-x/1.4)} + 20.8$ **[K2].**

and molecules in the lamp, as well as their interactions, there is a probability that each measurement cycle had slightly different „initial conditions" that determined the occurrence of self–modulation.

For voltages from 25 V to 29 V, the measurements exhibited good repeatability. The relative error at 25 V was 5%, and at other voltage values, it was approximately 10%. The accuracy of the voltage setting within ± 0.1 V and the possible current variations within ± 0.01 A influenced the resulting power at which the lamp operated each time.

3.5.5. Changes in line profiles during self–modulation

Changes in spectral line profiles were analyzed during several self–modulation periods to study how they change during the self–modulation regime.

For the description of work element spectral lines, the As 235.0 nm spectral line was chosen because it is intense and not a resonance spectral line, reducing the possibility of self–absorption.

For buffer gas spectral line description the Ar 763.5 nm spectral line was selected because it is intense and has been previously examined in this work.

The Gaussian half–width was calculated using the *FitPeak* function in OriginPro 2019b software by fitting with a *Gaussian* function.

A comparison of the As 234.9 nm spectral line's integral intensities with its Gaussian half–width during a 1.5–minute self–modulation process at 27 V excitation generator voltage is shown in figure 3.14.

Comparing the changes in spectral line intensities during the cycle with changes in Gaussian half–widths over the corresponding time, it can be observed that during the spectral line intensity increase, the Gaussian half–width remains unchanged, but it changes immediately after the intensity drop. These changes overall indicate that the half–width initially decreases, then increases, and then returns to its average value in every pulse.

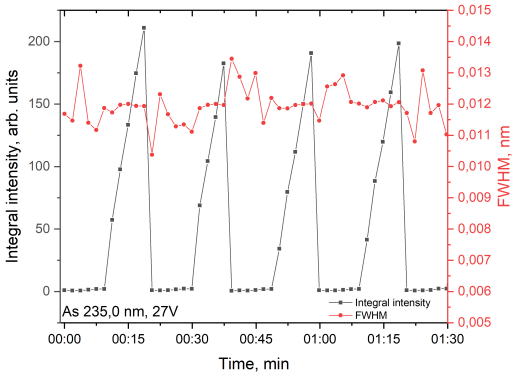

Figure 3.14: **Comparison of integral intensities and Gaussian half–width of As 235.0 nm spectral line during self–modulation process at 27 V excitation generator power.**

In figure 3.15, a comparison of changes in the Ar 763.5 nm spectral line intensity with changes in Gaussian half–width during a 1.5–minute self–modulation process at 27 V excitation generator voltage is shown.

In the case of argon, it can be observed that the spectral line half–width remains unchanged during the maximum phase of the pulse, but as the argon intensity decreases rapidly, the spectral line half–width also decreases.

Doppler broadening relates spectral line Gaussian half–width to temperature, but, in this case, temperature determination from the Gaussian half–widths for both arsenic and argon was not possible as the recorded spectral lines did not have sufficient resolution. However, changes in half–widths may be associated with temperature variations in the lamp. The observed changes in half–widths, specifically the decrease in the minimum phase, coincide with the expected temperature variations during the self–modulation process, as discussed in theory.

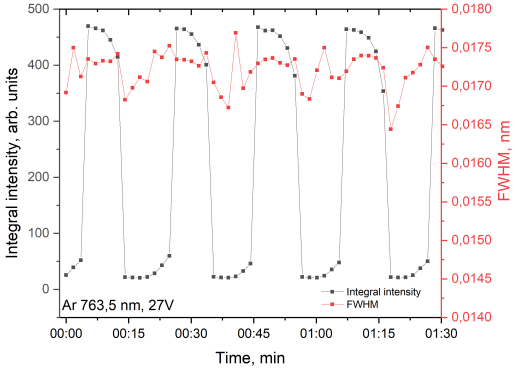

Figure 3.15: **Comparison of integral intensities and Gaussian half–width for Ar 763.5 nm spectral line during self–modulation process at 27 V excitation generator power.**

The relationship between temperature and self–modulation processes in high–frequency electrodeless lamps containing BiI_3 was described in the work by Zinge et al. [46]. In this work, it was calculated that the electron temperature varies from about 0.4 eV in the maximum phase to about 0.65 eV in the minimum phase [46]. Additionally, the change in rotational temperature during self–modulation in thallium HFEDL was examined in the work [41]. For temperature determination, the OH radical and the C_2 molecule were used. These results showed that the rotational temperature also varies periodically. The temperature change determined from OH radical during self–modulation was approximately 250 K [41].

3.6. Temperature determination using the distribution of OH radical rotational spectrum intensities

In several As HFEDLs, it was possible to observe the OH radical rotational spectrum lines in the 306 nm region for the $A^2\Sigma^+ \rightarrow X^2\Pi$ transition, which can be used for rotational temperature determination [P11]. A Jobin Yvon spectrometer was used for the registration of OH rotational molecular spectra.

In two of the As HFEDLs, spectral lines of OH rotational molecule were suitable for temperature determination (the spectral lines were sufficiently intense and did not overlap with other molecular spectral lines). Figure 1.3 was used for spectrum decryption.

To determine the plasma temperature, the intensities of the OH radical rotational spectrum Q_1 branch spectral lines $Q_1(4)$ – $Q_1(6)$ and $Q_1(8)$ – $Q_1(10)$ marked in figure 1.3 were first read from the recorded spectra.

Then, using the 1.6 formula and the values provided in table 1.1, the values of points for the Boltzmann semi–logarithmic graph for temperature determination were calculated. Each lamp had 8 values calculated for 8 different power values: for the L3 lamp from 14 to 21 W (figure 3.16 a)) and the L14 lamp from 13 to 20 W (figure 3.16 b)). From the graphs (figure 3.16), it can be seen that in most cases, the population distribution of As HFEDL by rotational levels follows the Boltzmann distribution only for the J=4, J=5, and J=6 levels (the first three points in each power group). Therefore, for temperature calculation, only the intensities of the $Q_1(4)$, $Q_1(5)$, and $Q_1(6)$ lines were used.

The respective calculated logarithm values of reduced intensities for $Q_1(4)$ – Q1(6) spectral lines were linearly approximated, and their slopes were determined. Since, according to equation 1.6, the slope value is equal to $\frac{-0.625}{Trot}$, temperature can be expressed and calculated from this equation.

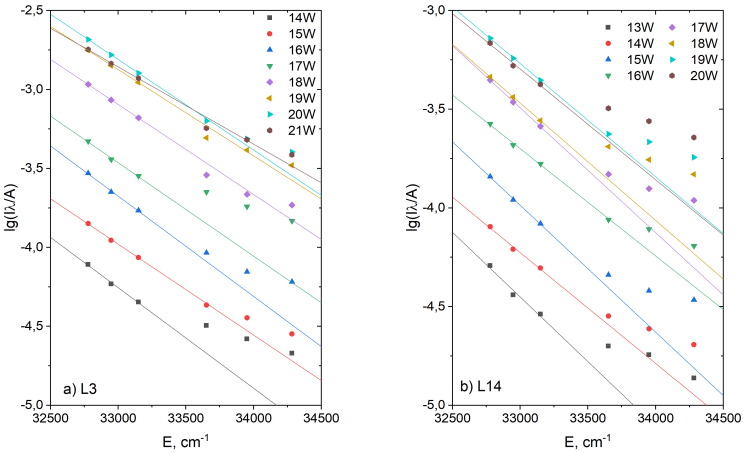

Figure 3.16: **Boltzmann semi–logarithmic graphs for OH (A–X (0–0)) Q_1 branch spectral lines in a) arsenic HFEDL number L3 b) arsenic HFEDL number L14 for different excitation generator power values.**

The obtained temperature values as a function of the input generator power are shown in figure 3.17. For the estimation of temperature errors, the standard deviations of the determined slopes of approximation lines were used.

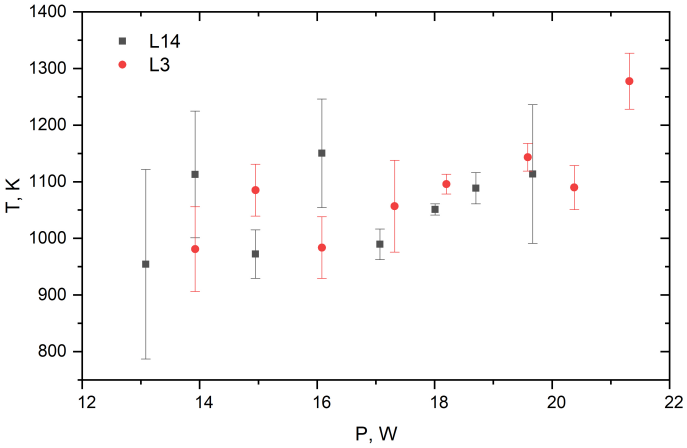

Figure 3.17: **Rotational temperature determined from OH radical rotational band (transition $A^2\Sigma^+ \rightarrow X^2\Pi$) Q–branch spectral lines in two As–containing HFEDLs (L3 and L14).**

It can be observed that the temperature increases in both lamps as the generator power increases.

In the L3 lamp, the temperature increases from 950 K at 14.0 W to 1250 K at 21.0 W. The temperature determination errors for this lamp do not exceed 8 %, with the largest errors occurring at 14.0 W and 17.3 W.

In the L14 lamp, the temperature increases from 950 K at 13.0 W to 1100 K at 19.7 W. Temperature determination errors for this lamp are 10 % or less, except at 13.1 W, where it is 18 %, and at 19.7 W, where the error is 11 %. The large error at low power levels could be explained by the low intensity of spectral lines.

This temperature range aligns with what has been observed in similar conditions in other high–frequency electrodeless lamps. For instance, in argon–hydrogen HFEDL, it increased from 650 K to 1100 K [P11], in thallium HFEDL from 820 K to 1060 K [41], and in mercury HFEDL, the temperature was determined to be in the range of 600 K to 1700 K [58].

4. Spectral measurements of mercury–containing high–frequency electrodeless lamps

In this work spherical and capillary mercury–containing high–frequency electrodeless lamps were studied. Spectral line intensities and stability were measured by Jobin Yvon spectrometer, but spectral line profiles were registered with Fourier spectrometer.

The main attention was given to the mercury resonance spectral line with a wavelength of 253.7 nm (transition $5d^{10}6s6p\ [^3P_1^o] \rightarrow 5d^{10}6s^2\ [^1S_0]$; transition probability A_{ik}=8, 4 · $10^6 s^{-1}$).

4.1. Hg capillary high–frequency electrodeless lamp

4.1.1. Influence of capillary on radiation spectra

In the case of capillary HFEDL, capillary position influences the spectrum of radiation [K7, K3]. Up to date, this phenomenon has been mainly studied in Hg spectral lines of visible light [59].

Hg capillary lamp can be positioned in three ways – with capillary horizontally (figure 4.1 a)), with capillary vertically and reservoir down (figure 4.1 b)), with capillary vertically and reservoir up (figure 4.1 c)).

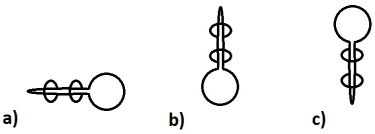

Figure 4.1: **Position of capillary: a) horizontally, b) vertically with the reservoir down, c) vertically with the reservoir up.**

Profiles of the Hg 253.7 nm spectral line in dependence of capillary position are shown in figure 4.2. The generator of capacitative excitation is supplemented with a magnet so it is possible to observe hyperfine splitting of spectral lines due to the Zeeman effect in magnetic field.

It can be seen that the highest radiation intensity is achieved when the lamp's capillary is positioned horizontally. The radiation from a vertically positioned capillary is several times lower, and higher intensity is observed when the lamp's reservoir is positioned upwards, while the radiation intensity is lowest when the reservoir is positioned downwards.

4.1.2. Stability of radiation

To assess the stability of the capillary HFEDL over time, changes in the intensity of the Hg 253.7 nm spectral line were recorded over half an hour, with the capillary positioned in each of the three positions: horizontally, with the reservoir up, and down. This allows for the simultaneous analysis of both radiation stability and the capillary's effect on radiation. The stability graphs for the spectral line are shown in figure 4.3.

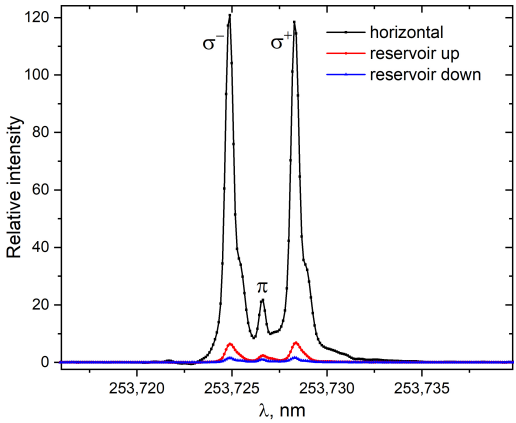

Figure 4.2: **Relative intensity and profile of Hg 253.7 nm spectral line in dependence on capillary position. Hyperfine splitting due to the Zeeman effect in a magnetic field can be observed [K3].**

As in the previous comparison, the highest radiation intensity is observed when the capillary is positioned horizontally. In this case, the radiation intensity fluctuated around the average value of 259 ± 5 relative units.

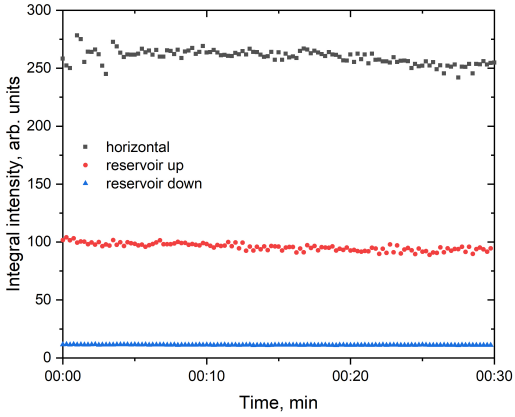

Figure 4.3: **Intensity changes of Hg 253.7 nm spectral line in capillary lamp in 30 min period. Measurements were done for three capillary positions – horizontal and vertical with reservoir either up or down.**

In contrast, for a vertically positioned capillary, it is several times smaller. When the reservoir is placed upwards, the radiation intensity is approximately 2.5 times lower than in the case of a horizontally positioned capillary and fluctuated around the average value of 96 ± 3 relative units. When the reservoir was positioned downwards, the radiation intensity was approximately 24 times lower than when the capillary was positioned horizontally and fluctuated around the average value of 11.2 ± 0.2 relative units.

The radiation is stable in all orientations. Intensity fluctuations for a horizontally positioned capillary were 2.1 %. When the lamp's reservoir was placed upwards, radiation fluctuations reached 3.1 %, and when the reservoir was down-

wards, it was 1.8 %. A horizontally positioned capillary lamp meets the conditions of a stable lamp [13].

It can be concluded that the most suitable orientation for the Hg capillary lamp is horizontal because in this case, the radiation is the most intense, while the least suitable orientation is with the capillary positioned vertically and the spherical reservoir downwards, as in this case, the signal–to–noise ratio, which is essential for AAS sensitivity, is the lowest.

4.2. Hg spherical high–frequency electrodeless lamp

4.2.1. Stability of radiation

Using the Jobin Yvon spectrometer, the 253.7 nm resonance spectral line intensity changes were recorded for 1 hour and 20 minutes for the mercury spherical HFEDL.

By integrating the spectral line intensity over its contour, it was observed that the integral intensity value remains stable over time once the lamp has warmed up, as shown in figure 4.4 a).

Because of the high resolution of the spectrometer, it was possible to observe that the line profile changes slightly over time, with a decrease in the line's maximum intensity and an increase in its width. The change in maximum intensity is shown in figure 4.4 b), while the change in spectral line half–width is shown in figure 4.4 c). Comparing both graphs, it can be seen that the change in maximum intensity is correlated with the change in half–width. This effect is related to temperature fluctuations in the lamp, as the lamp uses thermal insulation but is not temperature–controlled.

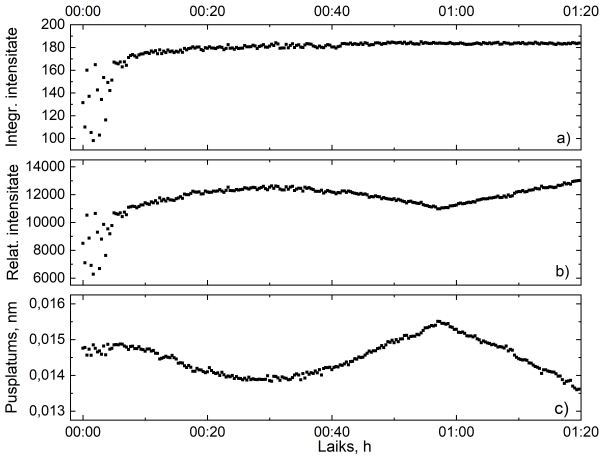

Figure 4.4: **Changes of Hg 253.7 nm spectral line during 1 h 20 min: a) for integrated intensity, b) for spectral line's max intensity, c) for spectral line's half–width.**

The integral intensity of the spectral line in the stable operating mode fluctuated around the average value of 182 relative units with a standard deviation of 2 units. Consequently, the intensity fluctuations were within the range of 1.1 %.

4.2.2. Radiation in E– and H–discharges

Hg 253.7 nm spectral line is very intense, so it can be studied both – in *E*–discharge and *H*–discharge.

Within the scope of the work, the relative intensity change of the Hg 253.7 nm spectral line was examined from 2.2 to 9.0 W of power, and the recorded integral spectral line intensities are shown in figure 4.5 a). It can be observed that the intensity of the 253.7 nm spectral line increases almost linearly from the power values of 2.2 to 4.8 W (corresponding to a voltage range of 9 to 14 V), followed by a sharp increase.

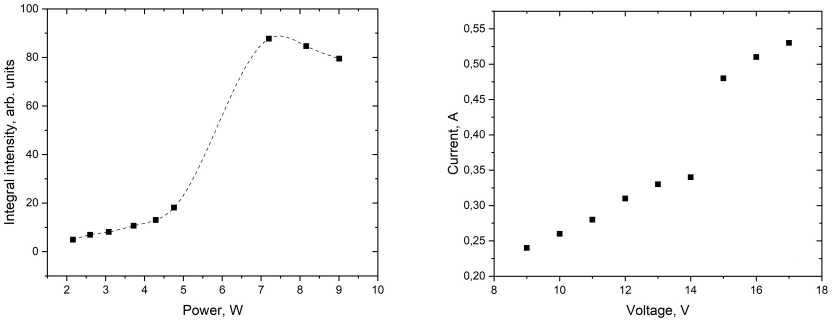

Figure 4.5: **a) Changes of integral intensity of Hg 253.7 nm spectral line depending on excitation generator power (in 2.2 – 9.0 W range).** Remark: experimentally obtained points are connected for better visuality only. **b) Current in dependence of voltage.**

It was observed that in this range at approximately 15 V voltage, there is a transition from *E*–discharge to *H*–discharge. For this reason, the graph shows both a rapid increase in intensity (on the y–axis) and a change in power values (on the x–axis) from 4.8 W at 14 V voltage to 7.2 W at 15 V voltage – when transitioning to *H*–discharge, the lamp's current also increases sharply (figure 4.5 b)), resulting in an increase in power. Following the jump, there is a gradual decrease in intensity at 7.2 to 9.0 W of power, which corresponds to a voltage range of 15 to 17 V.

Similar intensity changes are visible in figure 4.6, which shows how the profile of the Hg 253.7 nm spectral line changes depending on the power of the excitation generator, ranging from 2.6 to 9.0 W. The spectral line structure is also visible, which forms due to isotopic splitting in the lamp with a natural mercury mixture.

From 2.6 to 8.2 W, the intensity of the Hg spectral line increases, and in the power range from 5.3 to 8.2 W (corresponding to 15 – 16 V), there is a jump in intensity, transitioning from *E*–discharge to *H*–discharge. Afterward, from 8.2 to 9.0 W, a decrease in intensity is observed.

When evaluating the spectral line shape, it can be concluded that already at 5.3 W, self–absorption of the spectral line is visible, with a decrease in intensity

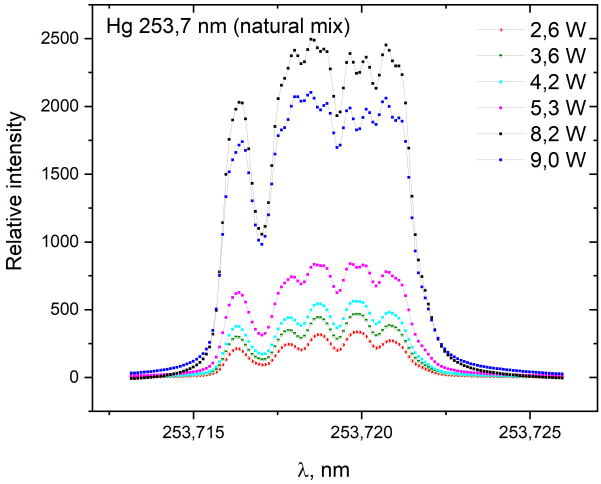

Figure 4.6: **Relative intensities of mercury 253.7 nm spectral line as a function of excitation generator power (from 2.6 W to 9.0 W). The spectral line splitting is visible due to isotopic composition and hyperfine structure.**

in the central part of the spectral line components. Self–absorption increases in *H*–discharge.

From this, it can be deduced that, unlike As HFEDL or Zn HFEDL (as mentioned in P8), which operate in *H*–discharge mode to achieve optimal spectral line intensity, it is recommended to operate Hg HFEDL in *E*–discharge mode to avoid self–absorption. An optimal power of approximately 3.6 to 4.2 W, corresponding to 12 – 13 V voltage, has to be chosen to ensure that the Hg 253.7 nm spectral line is not self–absorbed.

5. Comparison of high–frequency electrodeless lamps and hollow cathode lamps

The radiation of high–frequency electrodeless lamps containing arsenic and mercury were compared with respective hollow cathode lamps. To do it, spectra were recorded under identical conditions (lamp placement, environmental conditions, integration time while recording the radiation), and each lamp was operated within its respective optimal operating range. The optimal power range for HCLs was indicated in the lamp specifications given by the manufacturer.

Comparison of arsenic HFEDLs and HCLs

The spectrum of arsenic HFEDL was recorded in the power range from 12.4 to 18.8 W, corresponding to a voltage range of 21 to 27 V (current ranged from 0.59 to 0.70 A). The spectrum of As HCL was recorded in the power range from 1.2 to 2.6 W, corresponding to a current range of 5 to 9 mA (voltage varied between 246 and 289 V), with the manufacturer's recommended optimal current value being 7 mA and the maximum allowable current being 10 mA.

The integral intensities of the As 189.0 nm, 193.8 nm, and 197.3 nm spectral lines as a function of power for both lamps are shown in figure 5.1 a). An expanded graph of the integral intensities of As resonance spectral lines for HCL is shown in figure 5.1 b).

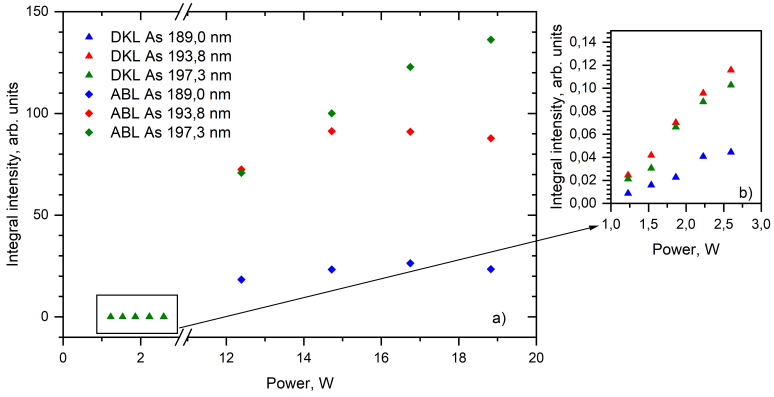

Figure 5.1: **Comparison of arsenic containing HFEDL and HCL: a) Integral intensities of As 189.0 nm, 193.8 nm and 197.3 nm spectral lines in HFEDL and HCL; b) zoomed–in graph part, showing integral intensities of As 189,0 nm, 193,8 nm and 197,3 nm spectral lines in HCL [K14].**

By comparing the intensities of all three As spectral lines in the two examined lamps, it is evident that in the high–frequency electrodeless lamp, they are much more intense. Assuming that the optimal operating power for HFEDL is approximately 15 W and for HCL it is around 2 W, the As spectral lines in HFEDL

are approximately 1000 to 1500 times more intense, depending on the selected spectral line.

Comparison of mercury HFEDLs and HCLs

The mercury HFEDL spectrum was recorded in the power range from 2.5 to 5.0 W, corresponding to a voltage range of 10 to 13 V (current ranged from 0.25 to 0.32 A). On the other hand, the Hg HCL spectrum was recorded in the power range from 0.6 to 1.6 W, corresponding to a current range of 3 to 7 mA (voltage varied between 194 and 233 V), with the manufacturer's recommended optimal current value being 5 mA and the maximum allowable current being 8 mA.

For comparing the intensities of mercury spectral lines, the resonance spectral line at 253.7 nm and a spectral line from the visible spectrum at 546.1 nm were used.

Both selected spectral line integral intensities as a function of power for both lamps are shown in figure 5.2 a). An expanded graph of Hg spectral line integral intensities specifically for HCL is shown in figure 5.2 b). Comparing the intensities of both Hg spectral lines in the two examined lamps, it is evident that the Hg spectral lines in HFEDL are considerably more intense.

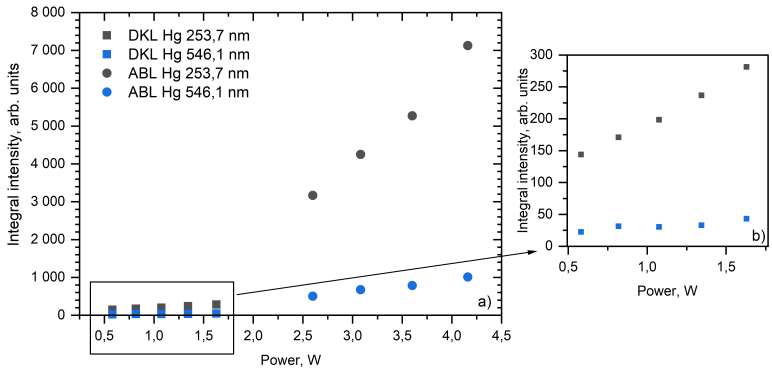

Figure 5.2: **Comparison of mercury containing HFEDL and HCL: a) Integral intensities of Hg 253.7 nm and 546.1 nm spectral lines in HFEDL and HCL; b) expanded graph part, showing integral intensities of Hg 253.7 nm and 546,1 nm spectral lines in HCL [K14].**

The given optimal operating power for Hg HFEDL is approximately 3.6 W, while for HCL, it is approximately 1.1 W. Comparing the Hg spectral line intensities at the optimal power values, it can be concluded that the Hg spectral line intensity in HFEDL is approximately 25 times greater than in HCL. Additionally, it should be noted that at an excitation generator power of 3.6 W, the mercury HFEDL operates in the *E*–discharge mode, but when transitioning to the *H*–discharge, the intensity of the Hg 253.7 nm spectral line increases by approximately 7 to 10 times (see section 4.2.2).

During the experiments with mercury–containing HCL, it stopped working. This indicates a short lamp lifetime.

6. Atomic absorption spectroscopy for mercury concentration measurements

This chapter gives insight into the practical use of atomic absorption spectrometer. An atomic absorption spectrometer with Zeeman background correction RA–915M was used to measure mercury concentration in environmental samples.

By adding an attachment for pyrolitic combustion PIRO–915+, it is possible to measure solid and liquid samples with the pyrolysis method [P1, P3, P4, K3, K4, K6, K10, K11, K13, K15].

The spectrometer can also be equipped with attachment RP–92, which allows measuring Hg concentration in liquid samples (mainly water), using the cold–vapor atomization method [P10, K15].

6.1. Mercury concentration measurements in black stork eggshells

This study used eggshells, that were gathered by Dr. Biol. Māris Strazds, during a period from 2003 to 2022.

6.1.1. Hg concentration in eggshells and membranes

A total of more than 350 black stork eggshell samples were analyzed from 139 nesting sites all over Latvia. After the separation of eggshells and inner membranes, 358 eggshells, 361 membranes, and 179 mixed samples were obtained. Sample gathering sites are shown on the map in figure 6.1.

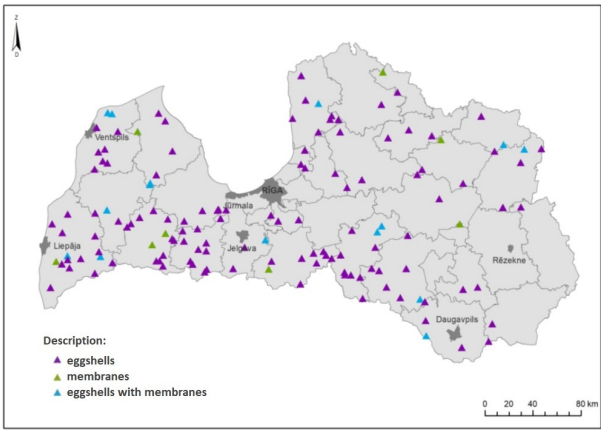

Figure 6.1: **Sample gathering sites for black stork eggshells and their membranes [60]. If several samples were obtained from one nesting site, eggshells are marked as the primary sample type.**

The measured mercury concentration in eggshells was from 3 to 52 ng/g, with an average value of 16 ng/g. In membranes, the average concentration was significantly higher – 202 ng/g, but most of the values were in the range of 43

– 815 ng/g. Selected membrane samples returned concentrations higher than 1000 ng/g [P3]. These high values are most likely explainable by egg yolk remaining stuck to the membranes, as the yolk contains even more mercury [53,54, 56]. Results and their distribution are shown in figure 6.2. Hg concentration in all analyzed samples was equal to or above the method's detection limit of 0.5 ng/g.

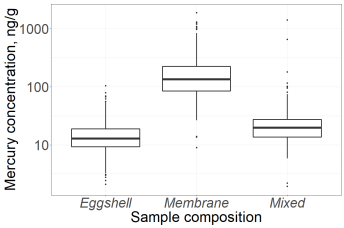

Figure 6.2: **Average Hg concentration in eggshell samples – eggshells, membranes, and mixed samples [P1].**

Mercury concentration is linked to the availability of mercury in the local environment within the foraging area of birds, and higher concentrations could indicate a local source of mercury or environmental contamination. However, it should be noted that black storks can travel up to 40 km from their nesting site in search of food [60].

Significant differences are observed between different parts of the egg, namely the membrane and the yolk. When comparing data from over 300 pairs of egg yolk and membrane samples, the average ratio of their mercury concentrations was 1:11, ranging from 1:4 to 1:30. This average value is close to what S. Peterson and colleagues found in their publication on mercury determination in American avocet egg yolks, which was 1:13.2 [55].

There are several possible explanations for the difference in mercury concentrations between egg yolks and membranes. One of them is the difference in chemical composition – egg yolks are more inorganic, while membranes are organic [61], and methylmercury, the primary form of mercury found in fish, tends to accumulate more in membranes. Another hypothesis involves the physiological formation of eggs – egg content first develops within the mother's body, and then the mineralization of the membrane occurs later [61]. Additionally, it is not known where mercury is located in the mother's body and how it is transferred to the eggs [P4].

6.1.2. Correlation estimation

Black storks in Latvia are an endangered species, and because of that only remains of hatched and failed eggs were collected. Available eggshells are different in size – from tiny scraps to almost whole eggshells, but sometimes there are only pieces of membranes without shells.

Because of the limited selection of samples, to obtain more thorough information, 320 sample pairs of eggshells and membranes were compared, to look for a correlation between them (figure 6.3). Since the sample sizes are small and

they do not follow a normal distribution, the mercury concentrations were natural log–transformed before conducting the statistical analysis. Data analysis was performed using the R software (version 4.2.1).

For characterizing the data distribution, Spearman's correlation analysis was chosen. A statistically significant positive correlation was obtained between membrane (C(HgM)) and yolk (C(HgCh)) concentrations (ρ=0.59; p–value < $2.2e^{-16}$), indicated by the correlation coefficient ρ exceeding 0.5. This implies that higher Hg concentrations in membranes are associated with higher Hg concentrations in egg yolks, and as shown in figure 6.3, the relationship is linear.

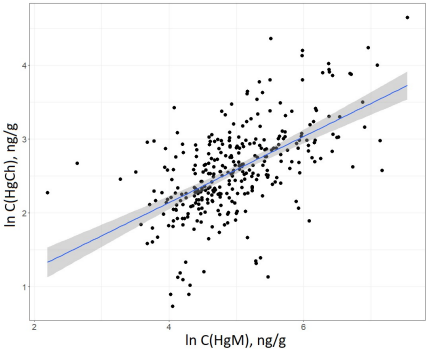

Figure 6.3: **Relation between log–transformed Hg concentrations in eggshells (C(HgCh)) and their membranes (C(HgM)). The correlation curve shows linear correlation, grey area indicates a 95% confidence region [P1].**

6.2. Hg concentration measurements in black stork feces

Feces are another way through which animals excrete pollutants from their bodies. By observing the behavior of black storks in their nest and vicinity, it has been discovered that adult birds cease constant vigilance over their chicks when the latter reach approximately 2 to 3 weeks of age. After this period (which is roughly at the beginning of June), adult birds no longer stay at the nest and only return to feed the nestlings. Consequently, it is possible to distinguish between the feces of adult birds (found near the nest in spring) and those of the chicks (collected during summer, after adult birds no longer defecate near the nest) [K10].

In the scope of this study, mercury concentration data were obtained from fecal samples collected from 2019 to 2022. In total, 201 samples were collected from 99 nesting sites. The distribution of samples by years and depending on the age of the birds – adults or chicks – is shown in table 6.1.

Figures 6.4 and 6.5 display graphs summarizing the mercury concentrations in feces obtained from samples collected in the spring and summer of 2021. The results are presented using unique nest identification numbers, which consist of six digits. Each nest has its distinctive number, which, along with the location name, date, and other archive information are used for sample identification.

Table 6.1:

Number of fecal samples distributed by year of collection and age of birds.

Year of collection	Nesting sites	Total N^o of samples	Feces, adult	Feces chick
2019	28	36	13	23
2020	31	41	22	19
2021	51	68	42	26
2022	42	56	30	26

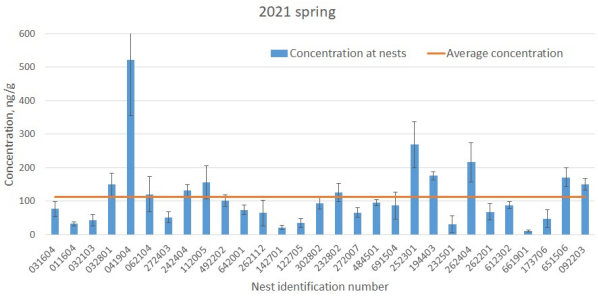

Figure 6.4: **Hg concentration in fecal samples gathered in the spring of 2021 [K6].The X–axis shows identification numbers for nesting sites.**

It can be observed that in the majority of samples, the Hg concentration ranges from 20 to 180 ng/g, with an average value of 110 ng/g. In some individual samples, the concentration exceeds 350 ng/g. The dispersion of Hg concentrations at each nesting site ranges from 3 to 50%, with three exceptions where it is higher than 50%. On average, the relative measurement error reaches 29%, which can be explained by the type and quantity of samples and the presence of vegetation residues in some samples, which can affect the final result. Within the

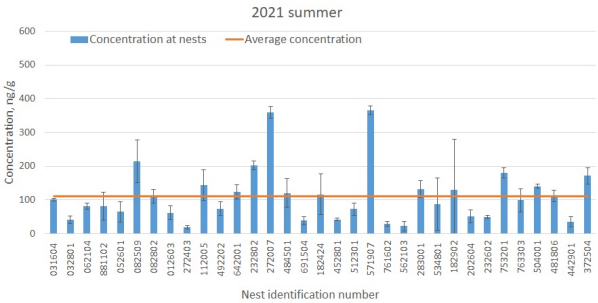

Figure 6.5: **Hg concentration in fecal samples gathered in the summer of 2021 [K6]. The X–axis shows identification numbers for nesting sites.**

limits of possibilities, the fecal samples were homogenized, but there is a possibility that Hg may not have been distributed evenly in the sample. The differences in Hg concentrations between nesting sites may indicate varying levels of Hg in

the surrounding environment. However, to draw such conclusions, data on the locations of nesting sites in regard to those of potential sources of mercury, river basins, and other feeding areas are needed.

A similar distribution of Hg concentrations among different nesting sites was also observed in samples from 2019, 2020, and 2022.

To examine trends in the average Hg concentrations in feces over several years, the average values for each year's summer and spring season samples were calculated. Accordingly, the average concentrations of samples from the spring and summer of 2019 to 2022 are shown in figure 6.6. A large concentration dispersion (the relative error is 50% – 80%) can be observed, which is related to the previously described concentration differences between nesting sites. At the same time, it is evident that the average Hg concentration fluctuates around 100 ng/g over the four–year period.

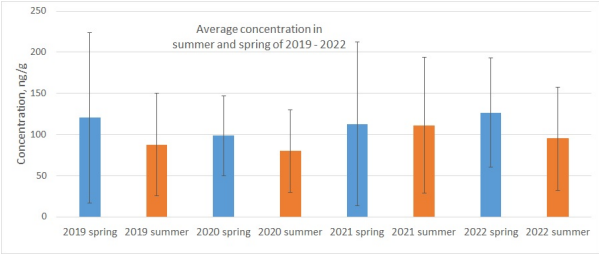

Figure 6.6: **Average Hg concentration in spring and summer samples for years 2019 – 2022 [K6].**

In the summer or chick feces, this value is lower than in spring or adult bird feces. This difference could be explained by the foraging locations and the age of the birds, as young birds typically receive food from the immediate area around the nest where their parents obtain it. Conversely, there is less information about the feeding areas of adult birds, and some of the mercury found in their feces may have come from a more polluted area, or it could be influenced by the mercury reserves in their bodies accumulated over time.

6.3. Hg measurements in solid samples by ZAAS – summary

Analyzing the methodology for Hg measurement and the obtained results, it can be concluded that the atomic absorption method coupled with Zeeman correction and sample atomization using pyrolysis is a convenient and relatively simple method for determining Hg concentrations in solid samples. The advantages of the method include the relatively simple preparation of samples, which reduces the risk of sample contamination during preparation. Additionally, dry samples are easier to store compared to solutions or frozen samples.

Challenges associated with the application of this method include the required quantity of the sample. Depending on the type and availability of samples to be measured, it may be sufficient, but sometimes too small to obtain accurate results. Problems can also arise if an organic sample generates smoke when

burned, which can hinder concentration determination during measurements by reducing the amount of light reaching the analyzer. Furthermore, if a sample generates residues when burned, these residues can deposit on the optical components of the analyzer, such as cuvette windows, contaminating them and reducing light transmission, thereby decreasing the sensitivity of the equipment. In such cases, frequent equipment cleaning is necessary.

A brief summary of the results of the measurements included in this work, including the type of samples, the number of samples, and the minimum, average, and maximum concentrations, is provided in table 6.2. Two groups of samples obtained from black storks were examined in this work – feathers, categorized into three subgroups (feathers, membranes, and mixed samples), and feces, categorized into two subgroups (adult bird and chick feces). The total number of analyzed samples exceeded 1000 units.

Table 6.2:

Brief summary of Hg concentrations in black stork samples.

		Concentration, ng/g		
Type of samples	N^o of samples	Average	Max	Min
Eggshells	358	16	105	3
Membranes	361	202	1880	9
Mixed samples	179	38	1411	7
Feces, adult	107	112	521	10
Feces, chick	94	110	366	8

The nearest legal norm in Latvia against which the obtained results can be compared is from Cabinet Regulation No. 118 [62], which states that the allowable concentration in biota is 20 μg/kg. This norm is primarily intended for the regulation of Hg concentrations in fish and is given in terms of wet weight. When comparing the obtained Hg concentrations, it should be considered that they were obtained in dry weight, so they would be lower in wet weight. The research found in literature [63] states that the conversion coefficient is approximately 4 – 5, meaning that the allowable norm in dry weight is around 80 – 100 μg/kg. By evaluating the results, it can be concluded that the average Hg concentration in eggshells is lower than the allowable norm, but in feces and membranes, it is at or exceeds the allowable norm.

Comparing the obtained Hg concentration results with the information found in the literature [27] regarding Hg concentration levels that can affect bird health and viability, it can be observed that in the majority of samples, the determined concentrations are low and do not pose a risk to the health and reproductive ability of black storks. However, in individual samples, measurement results reach levels (500 ng/g and higher, depending on the study, bird species, and type of sample examined) that could potentially affect the health and reproductive ability of storks.

6.4. Hg concentration measurements in water

The use of a Hg analyzer with Zeeman correction for measuring real natural water samples using the cold vapor method was evaluated in an international interlaboratory study organized by BrookRand Labs.

In the study on methods for measuring mercury concentrations, a total of 53 laboratories from 15 countries participated, with 49 providing data on total Hg concentration measurements and 36 on methylmercury concentration measurements [50]. Each laboratory received nine water samples with unknown Hg concentrations. After performing the measurements, the data were anonymously submitted to the study organizers, along with details of the sample preparation and measurement methods used. Since the actual concentrations in the samples were unknown, the submitted data were used to calculate mean values, and statistical data processing and analysis were conducted, as detailed in the study report [50].

The Hg concentration results obtained by me and my colleagues for each individual sample, as well as obtained mean values in accordance with the sampling location are shown in table 6.3. It can be observed that the results for all three sampling locations are slightly elevated compared to the overall mean concentrations. At the same time, they are close to the overall result obtained in the study, as indicated by the statistical indicators used in the study characterizing the results from Heron Pond and Sunset Pond as good.

Table 6.3:

Hg concentrations obtained in laboratory according to their sampling site and comparison with total average values, calculated from data provided by all participants of the study.

Sampling site	Heron Pond C_{Hg}, ng/l	Sunset Pond C_{Hg}, ng/l	Everett North C_{Hg}, ng/l
Results	6,5	6,6	1,9
	6,1	7,6	2,4
	8,1	6,4	0,8
Laboratory average	6,9	6,9	1,7
Total average	6,0	5,8	1,4

The Hg concentration values obtained in our laboratory for the Heron Pond sampling location compared to the data submitted by all other laboratories participating in the determination of total mercury concentrations are shown in Figure 6.7. The calculated mean Hg concentration of 6.0 ng/l is also marked on the graph. Comparing the results obtained by the laboratory with the results of other laboratories, it can be concluded that the chosen method and the mercury analyzer are suitable for measuring low mercury concentrations in water. Since the cold vapor method requires the use of chemicals and their solutions in sample preparation and measurement, attention must be paid to the purity of these substances in relation to mercury. It is also necessary to ensure the cleanliness of the laboratory vessels used in measurements.

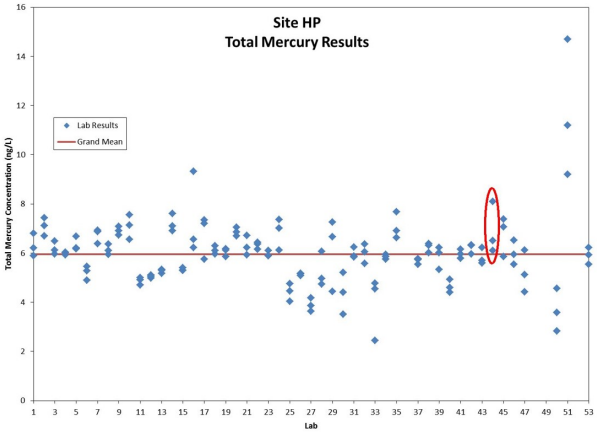

Figure 6.7: **Hg concentration results for all participants for sampling site Heron Pond, the red line indicates average value, but red ellipse encircles our results. Graph taken from study report [50].**

7. Conclusions

1. The optimal power for operating As HFEDL is approximately 14 W ($\approx$ 20 V) because at this power, there is no or minimal self–absorption of spectral lines. At higher power levels, self–absorption increases. The least self–absorbed was 197.3 nm spectral line, while the highest self–absorption and lowest intensity are observed for the 189.0 nm spectral line.

2. Using a 300 MHz frequency excitation generator results in higher intensity spectral lines at lower power compared to using a 100 MHz frequency generator.

3. Under certain conditions, arsenic–containing HFEDL transitions from stable mode to self–modulation mode. This transition typically occurs at an average excitation generator voltage of 26 – 28 V but can start as early as 24 V or not occur until up to 30 V. It was observed that adding a getter prevents the formation of self–modulation mode within the voltage range of 21 – 29 V. The self–modulation period of As HFEDL depends on the excitation generator power.

4. Long–term fluctuations in As HFEDL spectral lines are small, ranging from 0.3% to 0.7% depending on the lamp and operating conditions.

5. The gas temperature of As HFEDL is approximately 1000 – 1100 K. The obtained results are consistent with those obtained for HFEDLs of other elements.

6. Hg capillary lamps can be operated in three different positions – horizontally and vertically, with the reservoir up or down. The study results showed that the most suitable operating mode for the capillary lamp is with the capillary in a horizontal position. When evaluating the radiation stability for all three capillary positions, it was concluded that the horizontal and vertical with the reservoir down capillary positions provide the most stable radiation, with fluctuations of approximately 2%.

7. Hg spherical lamps operate in both the E–discharge and H–discharge modes, with the transition from one discharge to the other occurring at around 15 V. The optimal operating voltage for AAS is approximately 12 —13 V because at higher voltage values, spectral line self–absorption is observed. After stabilization, the radiation fluctuations for the Hg 253.7 nm spectral line in the spherical lamp reached 1.1%.

8. When comparing the spectra of As and Hg–containing HFEDLs with HCLs, HFEDLs provide significantly more intense radiation. The intensity of arsenic HFEDL spectral lines was up to 1000 times higher, while Hg HFEDL

had at least 25 times higher intensity compared to the corresponding spectral lines of HCL.

9. Zeeman AAS is a suitable method for determining Hg concentration in bird eggshells, membranes, and fecal samples, allowing measurements at around 5 ng/g. Using the pyrolysis method, sample preparation is minimal, reducing the risk of contamination, and results are obtained quickly, within a few minutes.

10. The concentration of mercury in eggshells is approximately 9 – 11 times lower than in membranes. In eggshells where the membrane is intact, mercury concentration is higher (average concentration 38 ng/g) than in those where the membranes have been removed (average concentration 16 ng/g). This should be taken into account when comparing data in publications on Hg in eggshells. The average concentration in pure membranes is 202 ng/g. There is a moderately strong positive correlation between Hg concentration in eggshells and membranes.

11. Differences in Hg concentration were observed between adult bird feces and chick feces. In chick feces, the average Hg concentration is lower (94 ng/g) than in adult stork feces (107 ng/g).

12. The obtained Hg concentrations in black stork samples are close to the permissible biota limit set by the Cabinet of Ministers. However, most of the samples did not reach concentrations described in the literature as causing serious health issues.

13. By adding a cold vapor generation attachment to the ZAAS spectrometer, it is possible to measure Hg in water with a detection limit of 0.5 ng/L. Water sample measurements were included in the inter–laboratory study. The obtained results are close to those reported by other laboratories, indicating that the method used is suitable for determining Hg concentrations in natural waters.

Bibliography

[1] J. Briffa et al., "Heavy metal pollution in the environment and their toxicological effects on humans," *Heliyon*, vol. 6, no. 9, p. e04691, 2020.

[2] H. Ali et al., "Environmental chemistry and ecotoxicology of hazardous heavy metals: Environmental persistence, toxicity, and bioaccumulation," *Journal of Chemistry*, vol. 2019, pp. 1–14, 2019.

[3] S. R. Koirtyohann, "A history of atomic absorption spectrometry," *Analytical Chemistry*, vol. 63, no. 21, pp. 1024A–1031A, 1991.

[4] S. Akman et al., "Atomic absorption spectroscopy," in *Food Toxicants Analysis*, pp. 637–665, Elsevier, 2007.

[5] A. Walsh, "The application of atomic absorption spectra to chemical analysis," *Spectrochimica Acta*, vol. 7, pp. 108–117, 1955.

[6] U.S. EPA, *Method 245.1: Determination of Mercury in Water by Cold Vapor Atomic Absorption Spectrometry.* Cincinnati, OH, revision 3.0 ed., 1994.

[7] A. Gałuszka et al., "Moving your laboratories to the field – advantages and limitations of the use of field portable instruments in environmental sample analysis," *Environmental Research*, vol. 140, pp. 593–603, 2015.

[8] Z. Lv et al., "Portable and miniature mercury analyzer using direct sampling inbuilt-metal ceramic electrothermal vaporization," *Analytica Chimica Acta*, vol. 1231, p. 340444, 2022.

[9] A. Ganeev et al., "High-frequency electrodeless discharge lamps for atomic absorption analysis," *Spectrochimica Acta Part B: Atomic Spectroscopy*, vol. 58, no. 5, pp. 879–889, 2003.

[10] G. Revalde, A. Skudra, "Optimization of mercury vapour pressure for high-frequency electrodeless light sources," *Journal of Physics D: Applied Physics*, vol. 31, no. 23, pp. 3343–3348, 1998.

[11] A. Skudra, J. Silinsh, G. Revalde, M. Berzinsh,, N. Zorina, "Nanoscale modification of glass surfaces in the light sources," in *First Latvian conference Nanomaterials and nanotechnologies, proceedings* (I. Zalite, J. Krastins, eds.), pp. 34 – 39, Institute of Inorganic Chemistry, Riga Technical University, 2005.

[12] G. Revalde et al., "Use of radiation sources with mercury isotopes for real-time highly sensitive and selective benzene determination in air and natural gas by differential absorption spectrometry with the direct Zeeman effect," *Analytica Chimica Acta*, vol. 887, pp. 172–178, 2015.

[13] А. А. Пупышев, *Атомно-абсорбционный спектральный анализ [Atomic absorption spectral analysis]*. Мир химии, ТЕХНОСФЕРА, 2009. [In Russian].

[14] Agency for Toxic Substances and Disease Registry, "ATSDR's Substance Priority List." Online: https://www.atsdr.cdc.gov/spl/index.html. [Accessed 15.08.2023.].

[15] M. U. Rehman et al., “Fate of arsenic in living systems: Implications for sustainable and safe food chains,” *Journal of Hazardous Materials*, vol. 417, p. 126050, 2021.

[16] M. F. Hughes, B. D. Beck, Y. Chen, A. S. Lewis,, D. J. Thomas, “Arsenic exposure and toxicology: A historical perspective,” *Toxicological Sciences*, vol. 123, no. 2, pp. 305–332, 2011.

[17] F. Sprovieri et al., “Atmospheric mercury concentrations observed at ground-based monitoring sites globally distributed in the framework of the GMOS network,” *Atmospheric Chemistry and Physics*, vol. 16, no. 18, pp. 11915–11935, 2016.

[18] B. Gworek et al., “Mercury in the terrestrial environment: a review,” *Environmental Sciences Europe*, vol. 32, no. 1, 2020.

[19] B. Gworek et al., “Mercury in marine and oceanic waters – a review,” *Water, Air & Soil Pollution*, vol. 227, sep 2016.

[20] F. M. M. Morel et al., “The chemical cycle and bioaccumulation of mercury,” *Annual Review of Ecology and Systematics*, vol. 29, no. 1, pp. 543–566, 1998.

[21] R. A. Lavoie et al., “Biomagnification of mercury in aquatic food webs: A worldwide meta-analysis,” *Environmental Science & Technology*, vol. 47, no. 23, pp. 13385–13394, 2013.

[22] G. Harding et al., “Bioaccumulation of methylmercury within the marine food web of the outer Bay of Fundy, Gulf of Maine,” *PLOS ONE*, vol. 13, no. 7, p. e0197220, 2018.

[23] A. Skudra et al., “Alternative UV light sources for surface disinfection,” *ENVIRONMENT. TECHNOLOGIES. RESOURCES. Proceedings of the International Scientific and Practical Conference*, vol. 1, pp. 218–222, 2021.

[24] A. Skudra et al., “UV inactivation of Semliki Forest virus and bacteria by alternative light sources,” *Journal of Photochemistry and Photobiology*, vol. 10, p. 100120, 2022.

[25] J. Černova, “Ekoloģiskā piesārņojuma kumulācija melnā stārķa (Ciconia nigra) organismā [Cumulation of ecological pollution in black stork (Ciconia nigra) organism],” intern report, Latvijas Lauksaimniecības Universitāte, Jelgava, 2015. [In Latvian].

[26] V. Ķerus et al., *Latvijas ligzdojošo putnu atlanti 1980–2017 [Latvian Breeding Bird Atlases 1980–2017]*. Rīga: Latvijas Ornitoloģijas biedrība, 2021.

[27] J. T. Ackerman et al., “Avian mercury exposure and toxicological risk across western North America: A synthesis,” *Science of The Total Environment*, vol. 568, pp. 749–769, 2016.

[28] M. Kamiński et al., “Intra-seasonal and brood-size dependent variation in the diet of black stork (*Ciconia nigra*) nestlings,” *Waterbirds*, vol. 41, no. 3, pp. 268–275, 2018.

[29] C. A. Eagles-Smith et al., “Mercury bioaccumulation and risk to three waterbird foraging guilds is influenced by foraging ecology and breeding stage,” *Environmental Pollution*, vol. 157, no. 7, pp. 1993–2002, 2009.

[30] J. C. V. Loon, *Analytical atomic absorption spectroscopy*. Academic Press, 1980.

[31] S. A. Kazantsev et al., *Practical Spectroscopy of High-Frequency Discharges*. Springer New York, NY, 1998.

[32] S. Sholupov et al., “Zeeman AA monitors for determination of background mercury concentration in ambient air and gases without absorption traps,” in *Proceedings of 15th International Conference on Heavy Metals in the Environment*, p. 1071, Gdansk University of Technology, Gdansk: Poland, 2010.

[33] G. Revalde, “Spectral line modelling,” *Latvijas Universitātes Zinātniskie raksti*, vol. 573, pp. 44–52, 1992. [In Russian].

[34] G. Revalde et al., “Diagnostics of capillary mercury–argon high-frequency electrodeless discharge using line shapes,” *Journal of Quantitative Spectroscopy and Radiative Transfer*, vol. 94, no. 3-4, pp. 311–324, 2005.

[35] G. Revalde et al., “Investigation of Hg resonance 184.9nm line profile in a low–pressure mercury–argon discharge,” *Journal of Quantitative Spectroscopy and Radiative Transfer*, vol. 107, no. 1, pp. 164–172, 2007.

[36] N. Zorina et al., “Deconvolution of the mercury 253.7 nm spectral line shape for the use in absorption spectroscopy,” in *SPIE Proceedings* (J. Spigulis et al., eds.), SPIE, 2008.

[37] H. R. Griem, *Principles of Plasma Spectroscopy*. Cambridge University Press, 1997.

[38] S. J. Hill, ed., *Inductively coupled plasma spectrometry and its applications*. Blackwell Pub., 2. ed., 2006.

[39] C. O. Laux et al., “Optical diagnostics of atmospheric pressure air plasmas,” *Plasma Sources Science and Technology*, vol. 12, no. 2, pp. 125–138, 2003.

[40] N. Idris et al., “Temperature estimation using Boltzmann plot method of many calcium emission lines in laser plasma produced on river clamshell sample,” *Journal of Physics: Conference Series*, vol. 1120, p. 012098, nov 2018.

[41] M. Zinge et al., “Spectroscopic studies of Tl containing high frequency electrodeless lamps,” in *Proceedings of SPIE, Eighth International Conference on Advanced Optical Materials and Devices (AOMD-8)* (J. Spigulis, ed.), Vol. 9421, pp. 104 – 111, SPIE, 2014.

[42] V. N. Ochkin, *Spectroscopy Of Low Temperature Plasma*. Wiley–VCH Verlag GmbH, 2009.

[43] C. Engelhard et al., “Plasma diagnostic on a low-flow plasma for inductively coupled plasma optical emission spectrometry,” *Spectrochimica Acta Part B: Atomic Spectroscopy*, vol. 63, no. 6, pp. 619–629, 2008.

[44] U. Engel et al., “Spatially resolved measurements and plasma tomography with respect to the rotational temperatures for a microwave plasma torch,” *Journal of Analytical Atomic Spectrometry*, vol. 13, no. 9, pp. 955–961, 1998.

[45] К. Курейчик et al., *Газоразрядные источники света для спектральных измерений [Gas–discharge light sources for spectral measurements]*. Издательство ”Университетское”, Минск, 1987. [In Russian].

[46] M. Zinge et al., “Electron temperature determination of bismuth containing electrodelless light sources during self-modulation regime,” *Rom. Rep. Phys.*, vol. 71, no. 1 (404), pp. 1–10, 2019.

[47] W. S. Gleason, R. Pertel, “High stability electrodeless discharge lamps,” *Review of Scientific Instruments*, vol. 42, no. 11, pp. 1638–1643, 1971.

[48] A. Kramida, Y. Ralchenko, J. Reader,, NIST ASD Team, “NIST Atomic Spectra Database (ver. 5.10).” Online: https://www.nist.gov/pml/atomic-spectra-database, 2022. [Accessed 15.08.2023.].

[49] Lumex, *RA-915M Mercury Analyzer, operation manual*.

[50] J. Creswell et al., “2012 Brook Rand Labs Interlaboratory Comparison Study for Total Mercury and Methylmercury (Intercomp 2012),” interlaboratory comparison study, Brook Rand Labs, 2012.

[51] S. Kahle, P. H. Becker, “Bird blood as bioindicator for mercury in the environment,” *Chemosphere*, vol. 39, no. 14, pp. 2451–2457, 1999.

[52] K. Kucharska et al., “Spatial and temporal trends in mercury levels in the down of black stork chicks in central Europe,” *Environmental Pollution*, vol. 274, p. 116571, 2021.

[53] A. Aliakbari et al., “Mercury in egg and eggshell of Whiskered Tern (Chlidonias hybrida) from Anzali Wetlands of the Caspian Sea, Iran,” *Bulletin of Environmental Contamination and Toxicology*, vol. 86, no. 2, pp. 175–179, 2010.

[54] R. A. Kennamer et al., “Mercury patterns in wood duck eggs from contaminated reservoir in South Carolina, USA,” *Environmental Toxicology and Chemistry*, vol. 24, no. 7, p. 1793, 2005.

[55] S. H. Peterson et al., “A critical evaluation of the utility of eggshells for estimating mercury concentrations in avian eggs,” *Environmental Toxicology and Chemistry*, vol. 36, no. 9, pp. 2417–2427, 2017.

[56] R. L. Brasso et al., “Pattern of mercury allocation into egg components is independent of dietary exposure in Gentoo Penguins,” *Archives of Environmental Contamination and Toxicology*, vol. 62, no. 3, pp. 494–501, 2011.

[57] D. C. Evers et al., “Patterns and interpretation of mercury exposure in freshwater avian communities in northeastern North America,” *Ecotoxicology*, vol. 14, no. 1-2, pp. 193–221, 2005.

[58] N. Zorina, “Deconvolution of the spectral line profiles for the plasma temperature estimation,” *Nuclear Instruments and Methods in Physics Research*

Section A: Accelerators, Spectrometers, Detectors and Associated Equipment, vol. 623, no. 2, pp. 763–765, 2010.
[59] A. Skudra et al., "Spectroscopic diagnostics of mercury–containing capillary light sources for AAS," in *Abstracts of 11th International Conference on Mercury as a Global Pollutant*, 2013.
[60] Z. Brike, "Piesārņojuma ar dzīvsudrabu novērtējums melnajos stārķos (Ciconia nigra) Latvijā [Assessment of mercury pollution in black storks (Ciconia nigra)]," master thesis, Latvijas Universitāte, 2022. [In Latvian].
[61] R. G. Board, R. Fuller, eds., *Microbiology of the avian egg*. London, UK: Chapman & Hall, 1994.
[62] Cabinet of Ministers, "Cabinet Regulation Nr.118 Regulations Regarding the Quality of Surface Waters and Groundwaters." Online: https://likumi.lv/ta/id/60829-noteikumi-par-virszemes-un-pazemes-udenu-kvalitati. [Accessed 15.08.2023.].
[63] P. Cresson, M. Travers-Trolet, M. Rouquette, C.-A. Timmerman, C. Giraldo, S. Lefebvre,, B. Ernande, "Underestimation of chemical contamination in marine fish muscle tissue can be reduced by considering variable wet:dry weight ratios," *Marine Pollution Bulletin*, vol. 123, no. 1-2, pp. 279–285, 2017.

Acknowledgements

I would like to express my deepest gratitude to everyone involved in the creation of my doctoral thesis, especially:

- my supervisors Atis Skudra and Gita Rēvalde;
- Nataļja Zorina, Rita Veilande, Zanda Briķe, Zandai Gavare, Madara Ziņģe, Antonijai Rimša;
- Māris Strazds, Māris Tamanis and other colleagues.

Also many thanks to my family and friends for support and encouragement.